INTERNATIONAL JOURNAL FOR NUMERICAL METHODS IN ENGINEERING
Int. J. Numer. Meth. Engng 2008; **76**:1250–1279
Published online 28 April 2008 in Wiley InterScience (www.interscience.wiley.com). DOI: 10.1002/nme.2369

On the computation of the coupled thermo-electromagnetic response of continua with particulate microstructure

T. I. Zohdi*, †

Department of Mechanical Engineering, University of California, Berkeley, CA 94720-1740, U.S.A.

SUMMARY

Recently, several applications, primarily driven by micro-technology, have emerged where the use of materials with tailored electromagnetic properties is necessary for a successful design. The 'tailored' properties are achieved by doping an easily moldable base matrix with particles having dielectric constants that are chosen to give overall desired properties. In many cases, the analysis of such materials requires the simulation of the macroscopic and microscopic electromagnetic response, as well as its resulting coupled thermal response, which can be important to determine possible failure in 'hot spots'. In this study, a model and a solution strategy are developed to compute the response of a class of fully coupled electro-magneto-thermal systems composed of heterogeneous materials, involving the absorption of electromagnetic energy, its conversion to heat and changes in the electromagnetic material properties. The algorithm involves recursive staggering, whose convergence is dependent on the discretized time-step size. The multifield system coupling can change, becoming weaker, stronger or alternating back and forth. Therefore, it is quite difficult to determine *a priori* the time-step size needed to meet a prespecified tolerance on the staggering error, i.e. the incomplete resolution of the coupling between the fields. The presented solution process involves time-step size adaptivity to control the contraction mapping constant of the multifield system operator in order to induce desired staggering rates of convergence within each time step and to control the staggering error. Three-dimensional numerical experiments are performed to illustrate the behavior of the model and the solution strategy. Copyright © 2008 John Wiley & Sons, Ltd.

Received 13 February 2008; Revised 12 March 2008; Accepted 14 March 2008

KEY WORDS: effective electromagnetic properties; particulates

1. INTRODUCTION

Most modern electromagnetic devices owe a significant amount of their success to the tailored electromagnetic material behavior of the components that comprise them. A relatively inexpensive way to obtain macroscopically desired responses is to enhance an easy-to-form matrix material's

*Correspondence to: T. I. Zohdi, Department of Mechanical Engineering, University of California, Berkeley, CA 94720-1740, U.S.A.
†E-mail: zohdi@me.berkeley.edu

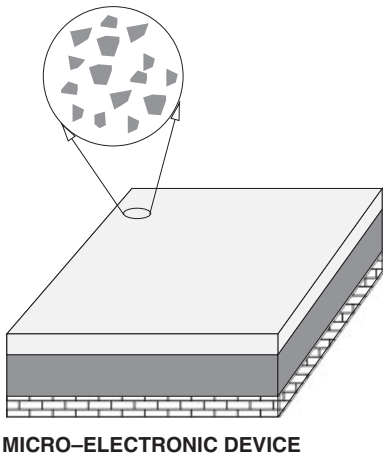

Figure 1. A microelectronic device with tailored layers.

properties by introducing microscale particles (Figure 1). The particles are chosen to produce an overall desired electromagnetic effect. The aggregate response of the material is an outcome of the interaction between the smaller-scale (microstructure) constituents that comprise the 'effective' material. In the construction of such materials, the basic philosophy is to select matrix/particle material combinations in order to produce desired aggregate responses. For example, in electromagnetic engineering applications, the classical choice is to add a particulate phase with suitable dielectric constants in order to modify the overall properties of a modable base matrix material.

Unfortunately, an attempt to directly simulate a device containing billions or even trillions of particles, incorporating all of the microscale details, requires an extremely fine spatial discretization mesh, for example, that of a finite difference or a finite element mesh, which is simply out of reach of virtually all computing devices in the foreseeable future. Furthermore, the exact subsurface geometry is typically impossible to ascertain throughout the structure. Essentially, a complete detailed solution of the entire device is nearly impossible. Fortunately, this type of analysis is usually unnecessary since, typically, an engineer wishes to know two primary things: (1) the effective or macroscale properties of the aggregate material and (2) the resulting thermal response of the material due to the absorption of the electromagnetic energy in a statistically representative volume element (RVE).[‡]

The determination of effective properties of materials with heterogeneous microstructure has had a long history. In the context of electromagnetics, the properties of microheterogeneous materials are characterized by a spatially variable permittivity $\boldsymbol{\varepsilon}$. Typically, in order to characterize the (homogenized) effective macroscopic response of such materials, a relationship between averages

$$\langle \mathbf{D} \rangle_{\Omega} = \boldsymbol{\varepsilon}^* \cdot \langle \mathbf{E} \rangle_{\Omega} \tag{1}$$

is sought, where $\langle \cdot \rangle_{\Omega} \stackrel{\text{def}}{=} 1/|\Omega| \int_{\Omega} \cdot \, \mathrm{d}\Omega$ is the averaging operator, and $\mathbf{D}$ and $\mathbf{E}$ are the electric flux and electric field within a statistically RVE of volume $|\Omega|$. The quantity $\boldsymbol{\varepsilon}^*$ is known as the effective

[‡]The determination of the thermal response is often critical in ascertaining the failure of a device.

DOI: 10.1002/nme

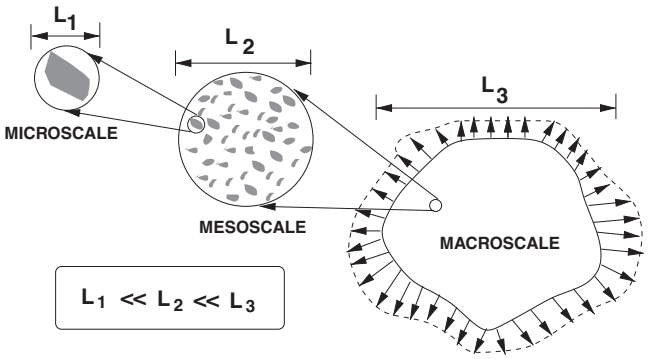

Figure 2. A representative sample of a material with heterogeneous microstructure.

permittivity property and is the permittivity tensor used in usual macroscale analyses. Similarly, one can describe other effective quantities such as

$$\langle \mathbf{B} \rangle_\Omega = \boldsymbol{\mu}^* \cdot \langle \mathbf{H} \rangle_\Omega \tag{2}$$

where $\mathbf{B}$ and $\mathbf{H}$ are the magnetic flux and magnetic field, and $\boldsymbol{\mu}^*$ is the effective magnetic permeability. For a sample to be statistically representative, it must usually contain a reasonably large number of particles (Figure 2); therefore, the computations over the RVE are still not trivial, but are of reduced computational effort in comparison with a direct attack on the entire macrostructural problem, if it were even possible.

Historically, because of the difficulties in computing effective properties directly, a variety of approximate techniques have been developed to estimate the overall macroscopic properties of materials consisting of a matrix containing distributions of particles.[§] In the realm of solid mechanics, Voigt [4] is usually cited with the first analysis of the linear effective *mechanical* properties of the microheterogeneous solids, $\langle \boldsymbol{\sigma} \rangle_\Omega = \mathbb{E}^* : \langle \boldsymbol{\varepsilon} \rangle_\Omega$, where $\boldsymbol{\sigma}$ is the stress and $\boldsymbol{\varepsilon}$ is the strain. Voigt approximated the strain field within an aggregate sample of heterogeneous material as being uniform, leading to $\langle \mathbb{E} \rangle_\Omega$ as an expression of the effective property. Reuss [5] approximated the stress fields within the aggregate of polycrystalline material as uniform, leading to $\langle \mathbb{E}^{-1} \rangle_\Omega^{-1}$ as an expression for the effective property. In 1952, Hill [6] proved that these assumptions provide bounds on the effective property, namely, $\langle \mathbb{E}^{-1} \rangle_\Omega^{-1} \leqslant \mathbb{E}^* \leqslant \langle \mathbb{E} \rangle_\Omega$. These inequalities mean that the eigenvalues of the tensors $\mathbb{E}^* - \langle \mathbb{E}^{-1} \rangle_\Omega^{-1}$ and $\langle \mathbb{E} \rangle_\Omega - \mathbb{E}^*$ are non-negative. One can interpret the Voigt and Reuss assumptions, and the resulting fields, as providing the extremes of possible behavior, since the Voigt stress field is one where the tractions at the phase boundaries cannot be in equilibrium (statically inadmissible), while the implied Reuss strains are such that the heterogeneities and the matrix could not be perfectly bonded, i.e. (kinematically inadmissible). These results can be easily re-interpreted for electrical and magnetic properties and fields to yield

$$\langle \boldsymbol{\varepsilon}^{-1} \rangle_\Omega^{-1} \leqslant \boldsymbol{\varepsilon}^* \leqslant \langle \boldsymbol{\varepsilon} \rangle_\Omega \tag{3}$$

[§] For example, see Maxwell [1, 2] and Rayleigh [3].

DOI: 10.1002/nme

where the upper bound is generated by assuming that the electric field is uniform throughout the medium and the lower bound is generated by assuming that the electric field flux is uniform throughout the medium. For the magnetic properties, one has

$$\langle \boldsymbol{\mu}^{-1} \rangle_{\Omega}^{-1} \leqslant \boldsymbol{\mu}^{*} \leqslant \langle \boldsymbol{\mu} \rangle_{\Omega} \tag{4}$$

where the upper bound is generated by assuming that the magnetic field is uniform throughout the medium and the lower bound is generated by assuming that the magnetic field flux is uniform throughout the medium. In the electromagnetics literature, the bounds in Equations (3) and (4) are often referred to as the Wiener bounds [7]. These inequalities mean that the eigenvalues of the tensors $\boldsymbol{\varepsilon}^{*} - \langle \boldsymbol{\varepsilon}^{-1} \rangle_{\Omega}^{-1}$ and $\langle \boldsymbol{\varepsilon} \rangle_{\Omega} - \boldsymbol{\varepsilon}^{*}$ are non-negative. Typically, the bounds are quite wide and provide only rough qualitative information. Within the last 50 years improved estimates have been pursued, with a notable contribution being the Hashin–Shtrikman bounds [8–11].[¶] The objective of the present study is to provide basic models and numerical solution strategies to analyze the coupled response of such materials by *direct simulation* using standard laptop/desktop equipment. Numerical experiments are conducted to explore the behavior of models and solution schemes, and the results are checked against analytical bounds on the effective system response when this is possible.

2. EFFECTIVE PROPERTIES OF HETEROGENEOUS ELECTROMAGNETIC MEDIA

In order to introduce fundamental concepts pertaining to effective properties of electromagnetic media, we initially start with static, lossless, conditions. Later, we consider more general, thermally sensitive, time-transient scenarios and the corresponding numerical methods. Let us start by simplifying the general formulations of Maxwell's equations, by simplifying Faraday's law for a static, lossless, case[‖]

$$\nabla \times \mathbf{E} = -\left(\frac{\partial (\boldsymbol{\mu} \cdot \mathbf{H})}{\partial t} + \mathbf{M}_{\mathrm{s}} + \hat{\boldsymbol{\sigma}} \cdot \mathbf{H} \right) \;\Rightarrow\; \nabla \times \mathbf{E} = \mathbf{0} \tag{5}$$

and Ampere's law

$$\nabla \times \mathbf{H} = \frac{\partial (\boldsymbol{\varepsilon} \cdot \mathbf{E})}{\partial t} + \mathbf{J}_{\mathrm{s}} + \boldsymbol{\sigma} \cdot \mathbf{E} \;\Rightarrow\; \nabla \times \mathbf{H} = \mathbf{0} \tag{6}$$

where $\mathbf{E}$ is the electric field intensity in V/m, $\mathbf{D}$ is the electric flux density in C/m^2, $\mathbf{J}$ is the electric current density in A/m^2, $\mathbf{H}$ is the magnetic field intensity in A/m, $\mathbf{B}$ is the magnetic flux density in Wb/m^2, $\mathbf{M}$ is the equivalent magnetic current density in V/m^2, $\boldsymbol{\varepsilon}$ is the electric permittivity in F/m, $\boldsymbol{\mu}$ is the magnetic permeability in H/m, $\boldsymbol{\sigma}$ is the electric conductivity in S/m and $\hat{\boldsymbol{\sigma}}$ is the

[¶] There exist several other approaches that seek to estimate or bound the aggregate responses of microheterogeneous materials. A complete survey is outside the scope of the present study. For a relatively recent and thorough analysis of a variety of classical approaches, such as those briefly mentioned here, see Torquato [12–16] for general interdisciplinary discussions, Jikov *et al.* [17] for more mathematical aspects, Aboudi [18], Hashin [11], Mura [19], Nemat-Nasser and Hori [20] for solid mechanics inclined accounts of the subject and Zohdi and Wriggers [21] for computational aspects.

[‖] Here, $\mathbf{M}_{\mathrm{s}}$ is an 'equivalent magnetic source' term and $\mathbf{J}_{\mathrm{s}}$ is a current source term.

DOI: 10.1002/nme

equivalent magnetic loss in Ω/m. Initially, we consider a simple effective property relationship between $\langle \mathbf{D} \rangle_\Omega$ and $\langle \mathbf{E} \rangle_\Omega$

$$\langle \mathbf{D} \rangle_\Omega = \boldsymbol{\varepsilon}^* \cdot \langle \mathbf{E} \rangle_\Omega \tag{7}$$

where $\boldsymbol{\varepsilon}^*$ is the effective permittivity. Similarly, we relate $\langle \mathbf{B} \rangle_\Omega$ and $\langle \mathbf{H} \rangle_\Omega$ by

$$\langle \mathbf{B} \rangle_\Omega = \boldsymbol{\mu}^* \cdot \langle \mathbf{H} \rangle_\Omega \tag{8}$$

where $\boldsymbol{\mu}^*$ is the effective magnetic permeability of the medium. As stated in the Introduction, it is clear that for the relationship between averages to be useful it must be computed over a sample containing a statistically representative amount of material.

2.1. Framing and the construction of a boundary value problem

A frequently used criterion for selecting sample sizes in effective property calculations is the well-known Hill condition [6]**

$$\langle \mathbf{D} \cdot \mathbf{E} \rangle_\Omega = \langle \mathbf{D} \rangle_\Omega \cdot \langle \mathbf{E} \rangle_\Omega \tag{9}$$

Basically, this is a statement that the micro-electrical-energy must equal the macro-electrical-energy. This is often referred to as an ergodicity condition in statistical mechanics. In order to understand the implications of Equation (9), we split the electric field flux and electric fields into a purely fluctuating (zero mean) $\mathbf{D} = \langle \mathbf{D} \rangle_\Omega + \tilde{\mathbf{D}}$, where $\langle \tilde{\mathbf{D}} \rangle_\Omega = \mathbf{0}$, and $\mathbf{E} = \langle \mathbf{E} \rangle_\Omega + \tilde{\mathbf{E}}$, where $\langle \tilde{\mathbf{E}} \rangle_\Omega = \mathbf{0}$; we obtain the following equation by direct expansion of the system energy:

$$\langle (\langle \mathbf{D} \rangle_\Omega + \tilde{\mathbf{D}}) \cdot (\langle \mathbf{E} \rangle_\Omega + \tilde{\mathbf{E}}) \rangle_\Omega = \langle \mathbf{D} \rangle_\Omega \cdot \langle \mathbf{E} \rangle_\Omega + \langle \tilde{\mathbf{D}} \cdot \tilde{\mathbf{E}} \rangle_\Omega \tag{10}$$

since $\langle \tilde{\mathbf{D}} \rangle_\Omega = \mathbf{0}$ and $\langle \tilde{\mathbf{E}} \rangle_\Omega = \mathbf{0}$. The ergodicity assumption is that $\langle \tilde{\mathbf{D}} \cdot \tilde{\mathbf{E}} \rangle_\Omega \to 0$, as $|\Omega| \to \infty$. The implication is that, as the sample becomes infinitely large, $\tilde{\mathbf{D}} \cdot \tilde{\mathbf{E}}$ is purely fluctuating and hence $\langle \tilde{\mathbf{D}} \cdot \tilde{\mathbf{E}} \rangle_\Omega = 0$. In other words, the product of two purely fluctuating random fields is also purely fluctuating. This is exactly the assertion of the Hill condition. Typically, an analyst will apply uniform loading on a large sample, with the understanding that this idealization 'mimics' what a RVE (which is much smaller than the structural component of intended use) would experience. It is clear that uniform loading is an idealization and, thus, will be present only within a vanishingly small microstructure relative to a finite-sized engineering (macro)structure.

The ergodicity assumption motivates the use of a 'framing' technique, which is a method whereby uniform far fields are applied on the boundary of a large sample, and the interior of the sample is then probed with subsamples, within the larger sample, in order to avoid boundary effects that occur from imposing the uniform fields on the larger sample exterior. This is akin to exploiting a St Venant type of effect, commonly used in solid mechanics, to avoid boundary layers. The approach provides a way of determining what the microstructure really experiences, without 'bias' from the boundary loading.

All of the following discussion holds for **B and **H**, in virtually the same manner. For more on ergodic hypotheses, see the classical work of Kröner [22].

DOI: 10.1002/nme

2.2. Computational testing

To determine $\boldsymbol{\varepsilon}^*$, one specifies three linearly independent (uniform) loadings of the form (1) $\mathbf{E}|_{\partial\Omega} = \mathscr{E}^{\mathrm{i}\to\mathrm{iii}}$ or (2) $\mathbf{D}|_{\partial\Omega} = \mathscr{D}^{\mathrm{i}\to\mathrm{iii}}$, where $\mathscr{E}^{\mathrm{i}\to\mathrm{iii}}$ and $\mathscr{D}^{\mathrm{i}\to\mathrm{iii}}$ are vectors with spatially constant components. This loading is applied to the sample in Figure 3, which depicts a microheterogeneous material. Each independent loading yields three different averaged electric field components and hence provides three equations for the constitutive constants in $\boldsymbol{\varepsilon}^*$. In order for such an analysis to be valid, i.e. to make the material data reliable, the sample must be small enough so that it can be considered as a material point with respect to the size of the domain under analysis, but large enough to be a statistically representative sample of the microstructure. In general, in order to determine the structural-scale material properties of microheterogeneous material one computes nine constitutive constants ε^*_{ij} in the following relationship between averages (actually six due to symmetry):

$$\begin{Bmatrix} \langle D_1\rangle_\Omega \\ \langle D_2\rangle_\Omega \\ \langle D_3\rangle_\Omega \end{Bmatrix} = \begin{bmatrix} \varepsilon^*_{11} & \varepsilon^*_{12} & \varepsilon^*_{13} \\ \varepsilon^*_{21} & \varepsilon^*_{22} & \varepsilon^*_{23} \\ \varepsilon^*_{31} & \varepsilon^*_{32} & \varepsilon^*_{33} \end{bmatrix} \begin{Bmatrix} \langle E_1\rangle_\Omega \\ \langle E_2\rangle_\Omega \\ \langle E_3\rangle_\Omega \end{Bmatrix} \tag{11}$$

As mentioned before, each independent loading leads to three equations and hence in total nine equations are generated by the three independent loadings, which are used to determine the tensor relationship between ($\boldsymbol{\varepsilon}^*$) average electric field flux and electric field. Note that $\boldsymbol{\varepsilon}^*$ *is exactly what appears in engineering books as the* '*property*' *of materials*. The usual choices for the three independent load cases are

$$\mathscr{E} \text{ or } \mathscr{D} = \begin{bmatrix} \beta \\ 0 \\ 0 \end{bmatrix}, \begin{bmatrix} 0 \\ \beta \\ 0 \end{bmatrix}, \begin{bmatrix} 0 \\ 0 \\ \beta \end{bmatrix} \tag{12}$$

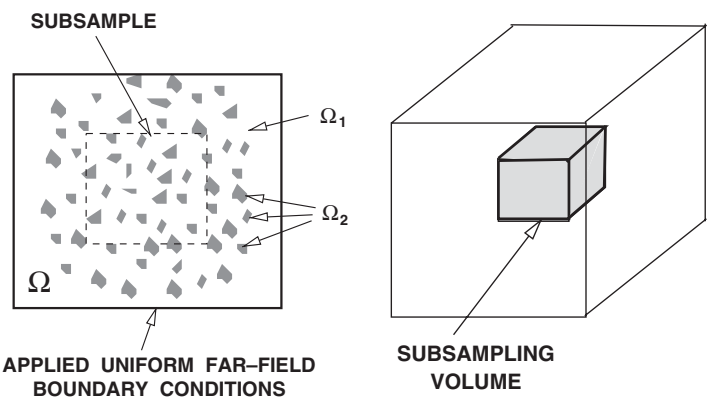

Figure 3. With the framing method, a sample is probed with interior subsamples, within the larger sample, in order to avoid boundary effects that occur from imposing the uniform fields on the large-sample exterior.

DOI: 10.1002/nme

where β is a 'load' parameter. Each independent loading state provides three equations, for a total of nine, which are used to determine the tensor ($\boldsymbol{\varepsilon}^*$) relationship between average electric field flux and electric field. The system of equations to be solved has the following form:

$$\begin{bmatrix} \langle E_1\rangle_\Omega^{\mathrm{i}} & \langle E_2\rangle_\Omega^{\mathrm{i}} & \langle E_3\rangle_\Omega^{\mathrm{i}} & 0 & 0 & 0 & 0 & 0 & 0 \\ 0 & 0 & 0 & \langle E_1\rangle_\Omega^{\mathrm{i}} & \langle E_2\rangle_\Omega^{\mathrm{i}} & \langle E_3\rangle_\Omega^{\mathrm{i}} & 0 & 0 & 0 \\ 0 & 0 & 0 & 0 & 0 & 0 & \langle E_1\rangle_\Omega^{\mathrm{i}} & \langle E_2\rangle_\Omega^{\mathrm{i}} & \langle E_3\rangle_\Omega^{\mathrm{i}} \\ \langle E_1\rangle_\Omega^{\mathrm{ii}} & \langle E_2\rangle_\Omega^{\mathrm{ii}} & \langle E_3\rangle_\Omega^{\mathrm{ii}} & 0 & 0 & 0 & 0 & 0 & 0 \\ 0 & 0 & 0 & \langle E_1\rangle_\Omega^{\mathrm{ii}} & \langle E_2\rangle_\Omega^{\mathrm{ii}} & \langle E_3\rangle_\Omega^{\mathrm{ii}} & 0 & 0 & 0 \\ 0 & 0 & 0 & 0 & 0 & 0 & \langle E_1\rangle_\Omega^{\mathrm{ii}} & \langle E_2\rangle_\Omega^{\mathrm{ii}} & \langle E_3\rangle_\Omega^{\mathrm{ii}} \\ \langle E_1\rangle_\Omega^{\mathrm{iii}} & \langle E_2\rangle_\Omega^{\mathrm{iii}} & \langle E_3\rangle_\Omega^{\mathrm{iii}} & 0 & 0 & 0 & 0 & 0 & 0 \\ 0 & 0 & 0 & \langle E_1\rangle_\Omega^{\mathrm{iii}} & \langle E_2\rangle_\Omega^{\mathrm{iii}} & \langle E_3\rangle_\Omega^{\mathrm{iii}} & 0 & 0 & 0 \\ 0 & 0 & 0 & 0 & 0 & 0 & \langle E_1\rangle_\Omega^{\mathrm{iii}} & \langle E_2\rangle_\Omega^{\mathrm{iii}} & \langle E_3\rangle_\Omega^{\mathrm{iii}} \end{bmatrix} \begin{Bmatrix} \varepsilon_{11}^* \\ \varepsilon_{12}^* \\ \varepsilon_{13}^* \\ \varepsilon_{21}^* \\ \varepsilon_{22}^* \\ \varepsilon_{23}^* \\ \varepsilon_{31}^* \\ \varepsilon_{32}^* \\ \varepsilon_{33}^* \end{Bmatrix} = \begin{Bmatrix} \langle D_1\rangle_\Omega^{\mathrm{i}} \\ \langle D_2\rangle_\Omega^{\mathrm{i}} \\ \langle D_3\rangle_\Omega^{\mathrm{i}} \\ \langle D_1\rangle_\Omega^{\mathrm{ii}} \\ \langle D_2\rangle_\Omega^{\mathrm{ii}} \\ \langle D_3\rangle_\Omega^{\mathrm{ii}} \\ \langle D_1\rangle_\Omega^{\mathrm{iii}} \\ \langle D_2\rangle_\Omega^{\mathrm{iii}} \\ \langle D_3\rangle_\Omega^{\mathrm{iii}} \end{Bmatrix} \tag{13}$$

Importantly, if the effective response is assumed to be isotropic, then only one test loading (instead of usually three) is required

$$\varepsilon^* \stackrel{\text{def}}{=} \sqrt{\frac{\langle \mathbf{D}\rangle_\Omega \cdot \langle \mathbf{D}\rangle_\Omega}{\langle \mathbf{E}\rangle_\Omega \cdot \langle \mathbf{E}\rangle_\Omega}} \tag{14}$$

with a similar relationship holding for

$$\mu^* \stackrel{\text{def}}{=} \sqrt{\frac{\langle \mathbf{B}\rangle_\Omega \cdot \langle \mathbf{B}\rangle_\Omega}{\langle \mathbf{H}\rangle_\Omega \cdot \langle \mathbf{H}\rangle_\Omega}} \tag{15}$$

Since we will be dealing with materials composed of randomly dispersed particulate media, we shall assume that the materials have an overall isotropic response and that Equations (14) and (15) are adequate to describe the effective material. We note that, even if the aggregate response is not purely isotropic, one can interpret the above expressions as approximations of isotropic responses.[††]

3. SOLUTION TO MAXWELL'S EQUATIONS

In order to generate the effective electromagnetic response of a heterogeneous continuum sample, we will need to solve Maxwell's equations posed over a representative sample domain. Our goal is to solve general formulations of Maxwell's equations over such a sample of material in order

[††]Applying uniform far fields on the boundary of a large sample is a way of attempting to reproduce the length-scale disparities that are necessary for the use of an effective property to make sense.

DOI: 10.1002/nme

to consider thermally sensitive, time-transient responses, by starting with Faraday's law

$$\nabla \times \mathbf{E} = -\left(\frac{\partial(\mu \mathbf{H})}{\partial t} + \mathbf{M}_s + \hat{\sigma}\mathbf{H} \right) \tag{16}$$

and Ampere's law

$$\nabla \times \mathbf{H} = \frac{\partial(\varepsilon \mathbf{E})}{\partial t} + \mathbf{J}_s + \sigma \mathbf{E} \tag{17}$$

where the material is assumed to be heterogeneous, and μ and ε are assumed to be (pointwise) isotropic (scalars) and time varying, due to the time-dependent thermal dependence, which is described shortly. Towards that end, we first discuss the general discretization scheme.[‡‡]

3.1. Temporally adaptive iterative methods

Implicit time-stepping methods, with time-step size adaptivity, built on approaches found in Zohdi [21, 23–34], will be used throughout the upcoming analysis. In order to introduce basic concepts, we consider a first-order differential equation (application to Maxwell's equations will follow)

$$\mathscr{M}\dot{\mathbf{W}} = \mathbf{F}(\mathbf{W}) \tag{18}$$

which, after being discretized using a trapezoidal 'ϕ-method' ($0 \leqslant \phi \leqslant 1$)

$$\mathbf{W}^{L+1} = \mathbf{W}^{L} + \frac{\Delta t}{\mathscr{M}}(\phi \mathbf{F}(\mathbf{W}^{L+1}) + (1-\phi)\mathbf{F}(\mathbf{W}^{L})) \tag{19}$$

yields the following abstract form:

$$\mathscr{A}(\mathbf{W}^{L+1}) = \mathscr{B} \tag{20}$$

It is convenient to express

$$\mathscr{A}(\mathbf{W}^{L+1}) - \mathscr{B} = \mathscr{G}(\mathbf{W}^{L+1}) - \mathbf{W}^{L+1} + \mathscr{R} = \mathbf{0} \tag{21}$$

where $\mathscr{R}$ is a remainder term that does not depend on the solution, i.e. $\mathscr{R} \neq \mathscr{R}(\mathbf{W}^{L+1})$. A straightforward iterative scheme can be expressed as

$$\mathbf{W}^{L+1,K} = \mathscr{G}(\mathbf{W}^{L+1,K-1}) + \mathscr{R} \tag{22}$$

where $K = 1, 2, 3, \ldots$ is the index of iteration within time step $L+1$. The convergence of such a scheme is dependent on the behavior of $\mathscr{G}$, namely, a sufficient condition for convergence is that $\mathscr{G}$ is a contraction mapping for all $\mathbf{W}^{L+1,K}$, $K = 1, 2, 3 \ldots$. In order to investigate this further, we define the iteration error as

$$\varpi^{L+1,K} \stackrel{\text{def}}{=} \mathbf{W}^{L+1,K} - \mathbf{W}^{L+1} \tag{23}$$

A necessary restriction for convergence is iterative self-consistency, i.e. the 'exact' (discretized) solution must be represented by the scheme

$$\mathscr{G}(\mathbf{W}^{L+1}) + \mathscr{R} = \mathbf{W}^{L+1} \tag{24}$$

[‡‡]The quantities σ and $\hat{\sigma}$ are assumed to be pointwise isotropic (scalars) as well.

DOI: 10.1002/nme

Enforcing this restriction, a sufficient condition for convergence is the existence of a contraction mapping

$$\varpi^{L+1,K} = \|\mathbf{W}^{L+1,K} - \mathbf{W}^{L+1}\| = \|\mathscr{G}(\mathbf{W}^{L+1,K-1}) - \mathscr{G}(\mathbf{W}^{L+1})\| \tag{25}$$

$$\leqslant \eta^{L+1,K} \|\mathbf{W}^{L+1,K-1} - \mathbf{W}^{L+1}\| \tag{26}$$

where if $0 \leqslant \eta^{L+1,K} < 1$ for each iteration K, then $\varpi^{L+1,K} \to \mathbf{0}$ for any arbitrary starting value $\mathbf{W}^{L+1,K=0}$, as $K \to \infty$. This type of contraction condition is sufficient, but not necessary, for convergence. Substituting these approximations into $\mathscr{M}\dot{\mathbf{W}} = \mathbf{F}(\mathbf{W})$ leads to

$$\mathbf{W}^{L+1,K} \approx \underbrace{\frac{\Delta t}{\mathscr{M}}(\phi \mathbf{F}(\mathbf{W}^{L+1}))}_{\mathscr{G}(\mathbf{W}^{L+1,K-1})} + \underbrace{\frac{\Delta t}{\mathscr{M}}(1-\phi)\mathbf{F}(\mathbf{W}^{L}) + \mathbf{W}^{L}}_{\mathscr{R}} \tag{27}$$

whose contraction constant is scaled by $\eta \propto \phi \Delta t / \mathscr{M}$. Therefore, we see that the contraction constant η is (1) directly dependent on the strength of the interaction forces, (2) inversely proportional to $\mathscr{M}$ and (3) directly proportional to $\phi \Delta t$ (at time=t). Therefore, if convergence is slow within a time step, the time-step size, which is adjustable, can be reduced by an appropriate amount to increase the rate of convergence. Decreasing the time-step size improves the convergence; however, we want to simultaneously maximize the time-step sizes to decrease the overall computing time, while still meeting an error tolerance on the numerical solution's accuracy. In order to achieve this goal, we follow an approach found in Zohdi [23, 24] originally developed for continuum thermo-chemical multifield problems in which one first approximates

$$\eta^{L+1,K} \approx S(\Delta t)^p \tag{28}$$

(S is a constant) and secondly one assumes the error within an iteration to behave according to

$$(S(\Delta t)^p)^K \varpi^{L+1,0} = \varpi^{L+1,K} \tag{29}$$

$K = 1, 2, \ldots$, where $\varpi^{L+1,0}$ is the initial norm of the iterative error and S is intrinsic to the system.[§§] Our goal is to meet an error tolerance in exactly a preset number of iterations. To this end, one expresses

$$(S(\Delta t_{\text{tol}})^p)^{K_{\text{d}}} \varpi^{L+1,0} = C_{\text{tol}} \tag{30}$$

where C_{tol} is a (coupling) tolerance and K_{d} is the number of desired iterations.[¶¶] If the error tolerance is not met in the desired number of iterations, the contraction constant $\eta^{L+1,K}$ is too large. Accordingly, one can solve for a new smaller step size, under the assumption that S is constant,

$$\Delta t_{\text{tol}} = \Delta t \left(\frac{(C_{\text{tol}}/\varpi^{L+1,0})^{1/pK_{\text{d}}}}{(\varpi^{L+1,K}/\varpi^{L+1,0})^{1/pK}} \right) \tag{31}$$

The assumption that S is constant is not critical, since the time steps are to be recursively refined and unrefined throughout the simulation. Clearly, the expression in Equation (31) can also be used for time-step enlargement, if convergence is met in less than K_{d} iterations.[‖‖]

[§§] For the class of problems under consideration, due to the quasi-linear dependency on Δt, $p \approx 1$.
[¶¶] Typically, K_{d} is chosen to be between 5 and 10 iterations.
[‖‖] At the implementation level, since the exact solution is unknown, the following relative error term is used, $\varpi^{L+1,K} \stackrel{\text{def}}{=} \mathbf{W}^{L+1,K} - \mathbf{W}^{L+1,K-1}$.

DOI: 10.1002/nme

Remarks

Obviously, we can use this scheme for any value of $0 \leqslant \phi \leqslant 1$. Time-step size adaptivity is important, since the solution can dramatically change over the course of time, possibly requiring quite different time-step sizes to control the staggering error. However, to maintain the accuracy of the time-stepping scheme, one must respect an upper bound dictated by the discretization error, i.e. $\Delta t \leqslant \Delta t^{\lim}$. Such an approach is highly advantageous since solutions to previous time steps can be used as the first guess to accelerate the solution procedure. A recursive iterative scheme of the Jacobi type, where the updates are made only after one complete system iteration, was illustrated here only for algebraic simplicity. The Jacobi method is easier to address theoretically, while the Gauss–Seidel-type method, which involves immediately using the most current values, when they become available, is used at the implementation level. It is important to realize that the Jacobi method is perfectly parallelizable. In other words, the update for each node is uncoupled, with the updates only coming afterward. Gauss–Seidel, since it requires the most current updates, couples the nodal calculations immediately. However, these methods can be combined to create hybrid approaches, whereby the entire domain is partitioned into subdomains and within each subdomain a Gauss–Seidel method is applied. In other words, for a subdomain, the values at any nodes from outside are initially frozen, as far as calculations involving members of the group are concerned. After each isolated group's solution (nodal values) has converged, computed in parallel, then all (interface) nodal values are updated, i.e. the most current values become available to all members of the grid, and the isolated subdomain calculations are repeated.

3.2. Electromagnetic algorithmic implementation

We now apply the introduced approach to electromagnetics. Let us start with a relatively general ('lossy') formulation of Maxwell's equations (Faraday's law and Ampere's law)

$$\frac{\partial(\mu\mathbf{H})}{\partial t} = -\nabla\times\mathbf{E} - \mathbf{M}_{\mathrm{s}} - \hat{\sigma}\mathbf{H} \stackrel{\mathrm{def}}{=} \mathbf{F} \tag{32}$$

and

$$\frac{\partial(\varepsilon\mathbf{E})}{\partial t} = \nabla\times\mathbf{H} - \mathbf{J}_{\mathrm{s}} - \sigma\mathbf{E} \stackrel{\mathrm{def}}{=} \mathbf{G} \tag{33}$$

We discretize for time $= t + \phi\Delta t$ and using a trapezoidal 'ϕ-scheme'

$$\frac{(\mu\mathbf{H})(t+\Delta t) - (\mu\mathbf{H})(t)}{\Delta t} \approx \mathbf{F}(t+\phi\Delta t) \approx \phi\mathbf{F}(t+\Delta t) + (1-\phi)\mathbf{F}(t) \tag{34}$$

and

$$\frac{(\varepsilon\mathbf{E})(t+\Delta t) - (\varepsilon\mathbf{E})(t)}{\Delta t} \approx \mathbf{G}(t+\phi\Delta t) \approx \phi\mathbf{G}(t+\Delta t) + (1-\phi)\mathbf{G}(t) \tag{35}$$

Rearranging yields

$$\mathbf{H}(t+\Delta t) \approx \frac{(\mu\mathbf{H})(t)}{\mu(t+\Delta t)} + \frac{\Delta t}{\mu(t+\Delta t)}(\phi\mathbf{F}(t+\Delta t) + (1-\phi)\mathbf{F}(t)) \tag{36}$$

and

$$\mathbf{E}(t+\Delta t) \approx \frac{(\varepsilon\mathbf{E})(t)}{\varepsilon(t+\Delta t)} + \frac{\Delta t}{\varepsilon(t+\Delta t)}(\phi\mathbf{G}(t+\Delta t) + (1-\phi)\mathbf{G}(t)) \tag{37}$$

DOI: 10.1002/nme

Numerically, the components of the gradient of functions such as $\mathbf{E}$ are approximated by central finite difference stencils of the form

$$\frac{\partial \mathbf{E}(x)}{\partial x} \approx \frac{\mathbf{E}(x+\Delta x)-\mathbf{E}(x-\Delta x)}{2\Delta x} \tag{38}$$

etc. In order to construct a solution, the algorithm is as follows:

(1) Construct derivative terms such as $\partial \mathbf{E}(x)/\partial x \approx \mathbf{E}(x+\Delta x)-\mathbf{E}(x-\Delta x)/2\Delta x$ for each node (i, j, k), $\mathbf{H}^{t+\Delta t} = \mathscr{F}(\mathbf{E}^{t+\Delta t}, \mathbf{H}^{t+\Delta t})$ and $\mathbf{E}^{t+\Delta t} = \mathscr{G}(\mathbf{E}^{t+\Delta t}, \mathbf{H}^{t+\Delta t})$.
(2) Compute $\mathbf{E}$-field with $\mathbf{H}$ fixed, then compute $\mathbf{H}$-field with $\mathbf{E}$ fixed, and iterate, $K = 1, 2\ldots$ for $\mathbf{H}^{t+\Delta t, K} = \mathscr{F}(\mathbf{E}^{t+\Delta t, K}, \mathbf{H}^{t+\Delta t, K-1})$ and $\mathbf{E}^{t+\Delta t, K} = \mathscr{G}(\mathbf{E}^{t+\Delta t, K-1}, \mathbf{H}^{t+\Delta t, K-1})$.
(3) Compute error measures: $\varpi_K^* \stackrel{\text{def}}{=} \max(\varpi_{E-K}, \varpi_{H-K})$, $i = 1, \ldots,$ nodes

$$\varpi_{K-E} \stackrel{\text{def}}{=} \frac{\sum_{i=1}^{N} \|\mathbf{E}_i^{L+1,K} - \mathbf{E}_i^{L+1,K-1}\|}{\sum_{i=1}^{N} \|\mathbf{E}_i^{L+1,K} - \mathbf{E}_i^{L}\|}, \quad \varpi_{K-H} \stackrel{\text{def}}{=} \frac{\sum_{i=1}^{N} \|\mathbf{H}_i^{L+1,K} - \mathbf{H}_i^{L+1,K-1}\|}{\sum_{i=1}^{N} \|\mathbf{H}_i^{L+1,K} - \mathbf{H}_i^{L}\|}$$

(4) If the tolerance is met, $\varpi^* \leqslant C_{\text{tol}}$ and $K \leqslant K_{\text{d}}$, then: (a) increment time forward: $t = t + \Delta t$, (b) construct new time step: $\Delta t = \Phi_K \Delta t$, where

$$\Phi_K \stackrel{\text{def}}{=} \left(\frac{(C_{\text{tol}}/\varpi_0^*)^{1/pK_{\text{d}}}}{(\varpi_K^*/\varpi_0^*)^{1/pK}} \right)$$

and (c) select $\Delta t = \min(\Delta t^{\text{lim}}, \Delta t)$ and go to (1).
(5) If the tolerance is not met, $\varpi^* > C_{\text{tol}}$ and $K = K_{\text{d}}$, then construct (refine) new time step: $\Delta t = \Phi_K \Delta t$ and go to (1).

At a given time, once the process is complete, then the time is incremented forward and the process is repeated. The overall goal is to deliver solutions where the iterative error is controlled and the temporal discretization accuracy dictates the upper limit on the time-step size (Δt^{lim}).

Remark 1
This type of iterative procedure is ideal for coupled problems, such as thermo-electromagnetic system, which we will treat shortly.

Remark 2
Although we will not employ explicit schemes, it is important to mention the most widely used type, the so-called Yee scheme [35]. A relatively clear exposition is given in Kunz and Luebbers [36] and Taflove and Hagness [37]. We remark that while the time-step size (associated with the Courant–Friedrichs–Levy (CFL) condition) is clearly one concern, an overriding one is stability, i.e. that errors at one time step do not grow in the next time step. We refer the reader to Taflove and Hagness [37] for a detailed discussion. The Yee method is subject to time-step restrictions due to stability issues and, since we shall iterate due to the use of multifield staggering schemes (introduced shortly with thermal coupling), implicit methods are preferred for the applications of interest.

DOI: 10.1002/nme

4. COUPLED THERMAL EFFECTS

4.1. The Poynting vector

Electromagnetic waves traveling through space carry energy that flows in the direction of wave propagation. The energy per unit area per unit time flowing into a surface in free space is given by the Poynting vector $\mathbf{S}=\mathbf{E}\times\mathbf{H}$. The Poynting vector has an intimate connection to the conservation of energy. To see this, form the inner product of the magnetic field with Faraday's law

$$\mathbf{H}\cdot(\nabla\times\mathbf{E})=-\mathbf{H}\cdot\left(\underbrace{\mathbf{M}_{\mathrm{s}}+\hat{\sigma}\mathbf{H}}_{\mathbf{M}}+\frac{\partial\mathbf{B}}{\partial t}\right) \tag{39}$$

and the inner product of the electric field with Ampere's law

$$\mathbf{E}\cdot(\nabla\times\mathbf{H})=\mathbf{E}\cdot\left(\underbrace{\mathbf{J}_{\mathrm{s}}+\sigma\mathbf{E}}_{\mathbf{J}}+\frac{\partial\mathbf{D}}{\partial t}\right) \tag{40}$$

Subtracting Equation (39) from Equation (40) yields

$$\underbrace{\mathbf{E}\cdot(\nabla\times\mathbf{H})-\mathbf{H}\cdot(\nabla\times\mathbf{E})}_{-\nabla\cdot(\mathbf{E}\times\mathbf{H})=-\nabla\cdot\mathbf{S}}=\mathbf{E}\cdot\mathbf{J}+\mathbf{H}\cdot\mathbf{M}+\underbrace{\mathbf{E}\cdot\frac{\partial\mathbf{D}}{\partial t}+\mathbf{H}\cdot\frac{\partial\mathbf{B}}{\partial t}}_{=\partial W/\partial t} \tag{41}$$

where W is the electromagnetic energy

$$W=\tfrac{1}{2}(\mathbf{E}\cdot\mathbf{D}+\mathbf{H}\cdot\mathbf{B})=\tfrac{1}{2}(\mathbf{E}\cdot\boldsymbol{\varepsilon}\cdot\mathbf{E}+\mathbf{H}\cdot\boldsymbol{\mu}\cdot\mathbf{H}) \tag{42}$$

Thus,

$$\nabla\cdot\mathbf{S}+\mathbf{E}\cdot\mathbf{J}+\mathbf{H}\cdot\mathbf{M}+\frac{\partial W}{\partial t}=0 \tag{43}$$

or

$$\frac{\partial W}{\partial t}=-\left(\nabla\cdot\mathbf{S}+\underbrace{\mathbf{E}\cdot\mathbf{J}+\mathbf{H}\cdot\mathbf{M}}_{\text{due to conduction}}\right) \tag{44}$$

Two main effects of the absorption of electromagnetic energy, which is converted into heat, are (a) thermally induced changes in the permittivity and permeability and (b) phase transformations. Both phenomena are controlled by the absorption of energy. In this study, we consider the absorbed energy that is available for heating to be proportional to the energy associated with conduction, namely, from Equation (44), $\mathbf{E}\cdot\mathbf{J}+\mathbf{H}\cdot\mathbf{M}$. In order to calculate the change in temperature, we must study the first law of thermodynamics. We consider that the deformation of the body, during all processes discussed in this monograph, is *negligible.* However, in keeping with the expository style, we derive a general case first, and then specialize it for our *zero-deformation* case.

DOI: 10.1002/nme

4.2. Absorption of energy

The interconversions of mechanical, thermal and electromagnetic energy in a system are governed by the first law of thermodynamics. It states that the time rate of change of the total energy, $\mathscr{K}+\mathscr{I}$, is equal to the work rate, $\mathscr{P}$, and the net heat supplied, $\mathscr{H}+\mathscr{Q}$,

$$\frac{\mathrm{d}}{\mathrm{d}t}(\mathscr{K}+\mathscr{I})=\mathscr{P}+\mathscr{H}+\mathscr{Q} \tag{45}$$

Here the kinetic energy of a subvolume of material contained in Ω, denoted as ω, is $\mathscr{K}\stackrel{\text{def}}{=}\int_\omega 1/2\rho\dot{\mathbf{u}}\cdot\dot{\mathbf{u}}\,\mathrm{d}\omega$; the rate of work or power of external forces acting on ω is given by $\mathscr{P}\stackrel{\text{def}}{=}\int_\omega \rho\mathbf{b}\cdot\dot{\mathbf{u}}\,\mathrm{d}\omega+\int_{\partial\omega}\mathbf{T}\cdot\mathbf{n}\cdot\dot{\mathbf{u}}\,\mathrm{d}a$, $\mathbf{T}$ being the Cauchy stress; $\mathbf{u}$ being the material displacement; the heat flow into the volume by conduction is $\mathscr{Q}\stackrel{\text{def}}{=}-\int_{\partial\omega}\mathbf{q}\cdot\mathbf{n}\,\mathrm{d}a=-\int_\omega\nabla_{\mathbf{x}}\cdot\mathbf{q}\,\mathrm{d}\omega$; the heat generated due to sources, *such as electromagnetic fields*, is $\mathscr{H}\stackrel{\text{def}}{=}\int_\omega \rho z\,\mathrm{d}\omega$ and the stored energy is $\mathscr{I}\stackrel{\text{def}}{=}\int_\omega \rho w\,\mathrm{d}\omega$. If we make the assumption that the mass in the system is constant, one has $\int_\omega\rho\,\mathrm{d}\omega=\int_{\omega_0}\rho J\,\mathrm{d}\omega_0=\int_{\omega_0}\rho_0\,\mathrm{d}\omega_0$, which implies that $\rho J=\rho_0$. Using this and the energy balance leads to

$$\begin{aligned}\frac{\mathrm{d}}{\mathrm{d}t}\int_\omega\frac{1}{2}\rho\dot{\mathbf{u}}\cdot\dot{\mathbf{u}}\,\mathrm{d}\omega&=\int_{\omega_0}\frac{\mathrm{d}}{\mathrm{d}t}\frac{1}{2}(\rho J\dot{\mathbf{u}}\cdot\dot{\mathbf{u}})\,\mathrm{d}\omega_0\\&=\int_{\omega_0}\left(\frac{\mathrm{d}}{\mathrm{d}t}\rho_0\right)\frac{1}{2}\dot{\mathbf{u}}\cdot\dot{\mathbf{u}}\,\mathrm{d}\omega_0+\int_\omega\rho\frac{\mathrm{d}}{\mathrm{d}t}\frac{1}{2}(\dot{\mathbf{u}}\cdot\dot{\mathbf{u}})\,\mathrm{d}\omega=\int_\omega\rho\dot{\mathbf{u}}\cdot\ddot{\mathbf{u}}\,\mathrm{d}\omega\end{aligned}$$

We also have

$$\frac{\mathrm{d}}{\mathrm{d}t}\int_\omega\rho w\,\mathrm{d}\omega=\frac{\mathrm{d}}{\mathrm{d}t}\int_{\omega_0}\rho J w\,\mathrm{d}\omega_0=\int_{\omega_0}\frac{\mathrm{d}}{\mathrm{d}t}(\rho_0)w\,\mathrm{d}\omega_0+\int_\omega\rho\dot{w}\,\mathrm{d}\omega \tag{46}$$

By using the divergence theorem, we obtain

$$\int_{\partial\omega}\mathbf{T}\cdot\mathbf{n}\cdot\dot{\mathbf{u}}\,\mathrm{d}a=\int_\omega\nabla_x\cdot(\mathbf{T}\cdot\dot{\mathbf{u}})\,\mathrm{d}\omega=\int_\omega(\nabla_x\cdot\mathbf{T})\cdot\dot{\mathbf{u}}\,\mathrm{d}\omega+\int_\omega\mathbf{T}:\nabla_x\dot{\mathbf{u}}\,\mathrm{d}\omega \tag{47}$$

Combining the results, and enforcing balance of momentum, leads to

$$\begin{aligned}&\int_\omega(\rho\dot{w}+\dot{\mathbf{u}}\cdot(\rho\ddot{\mathbf{u}}-\nabla_x\cdot\mathbf{T}-\rho\mathbf{b})-\mathbf{T}:\nabla_x\dot{\mathbf{u}}+\nabla_x\cdot\mathbf{q}-\rho z)\,\mathrm{d}\omega\\&=\int_\omega(\rho\dot{w}-\mathbf{T}:\nabla_x\dot{\mathbf{u}}+\nabla_x\cdot\mathbf{q}-\rho z)\,\mathrm{d}\omega=0\end{aligned} \tag{48}$$

Since the volume ω is arbitrary, the integrand must hold locally and we have

$$\rho\dot{w}-\mathbf{T}:\nabla_x\dot{\mathbf{u}}+\nabla_x\cdot\mathbf{q}-\rho z=0 \tag{49}$$

Note: In this monograph we do not consider the effects of (Cauchy) stress; thus, $\mathbf{T}=\mathbf{0}$. We assume $\dot{w}=C\dot{\theta}$; thus

$$\rho C\dot{\theta}=\nabla\cdot K\cdot\nabla\theta+\rho z \tag{50}$$

DOI: 10.1002/nme

where θ is the temperature in Kelvin, ρ is the density, C is the heat capacity, K is the conductivity and ρz is the rate of electromagnetic energy absorbed, namely

$$\rho z = a(\mathbf{E}\cdot\mathbf{J}+\mathbf{H}\cdot\mathbf{M}) \tag{51}$$

where a is an absorption constant, $0\leqslant a\leqslant 1$.

4.3. Thermal dependence of the material properties

The permittivity has a thermal dependence often modeled by

$$\varepsilon = \varepsilon_{\theta_0} e^{K_\varepsilon(\theta-\theta_0)} \tag{52}$$

and, similarly, for the permeability

$$\mu = \mu_{\theta_0} e^{K_\mu(\theta-\theta_0)} \tag{53}$$

where ε_{θ_0} and μ_{θ_0} are reference values at $\theta=\theta_0$.

4.4. Phase transformations

For phase transformations, we have four cases:

- *No melting*: If $\theta(t)<\theta_m$ and $\theta(t+\Delta t)<\theta_m$, then $C(\theta)=C_0$, where C_0 is the solid heat capacity.
- *Melting*: If $\theta(t)<\theta_m$ and $\theta(t+\Delta t)\geqslant\theta_m$, then $C(\theta)=C_0+\Delta H_m^{\mathrm{S}\to\mathrm{L}}/\Delta\theta_m$, where $\Delta H_m^{\mathrm{S}\to\mathrm{L}}$ is the latent heat of melting. This has the effect of enforcing a constant temperature (or absorbing the latent heat), where $\Delta\theta_m$ is small and can be thought of as a 'bandwidth' for melting.
- *Melted*: If $\theta(t)\geqslant\theta_m$ and $\theta(t+\Delta t)\geqslant\theta_m$, then $C(\theta)=C_m$, where C_m is the heat capacity of the melted material.
- *Solidification*: If $\theta(t)\geqslant\theta_m$ and $\theta(t+\Delta t)<\theta_m$, then $C(\theta)=C_m+\Delta H_m^{\mathrm{L}\to\mathrm{S}}/\Delta\theta_m$, where $\Delta H_m^{\mathrm{L}\to\mathrm{S}}$ is the latent heat of solidification.

4.5. Thermal discretization

Since we assume that there are no significant deformations, $\mathrm{d}/\mathrm{d}t=\partial/\partial t$ and the following approximation is made:

$$\frac{\partial\theta}{\partial t}\approx\frac{\theta(t+\Delta t)-\theta(t)}{\Delta t} \tag{54}$$

and

$$q\left(x+\frac{\Delta x}{2}\right)\approx -K\frac{\partial\theta}{\partial x}\approx -K\left(x+\frac{\Delta x}{2}\right)\frac{\theta(x+\Delta x)-\theta(x)}{\Delta x} \tag{55}$$

and

$$\frac{\partial q}{\partial x}\approx\frac{q\,(x+\Delta x/2)-q\,(x-\Delta x/2)}{\Delta x} \tag{56}$$

DOI: 10.1002/nme

therefore,

$$\frac{q\,(x+\Delta x/2)-q\,(x-\Delta x/2)}{\Delta x}$$
$$\approx -\frac{(K\,(x+\Delta x/2)\,(\theta(x+\Delta x)-\theta(x))-K\,(x-\Delta x/2)\,(\theta(x)-\theta(x-\Delta x)))}{(\Delta x)^2} \tag{57}$$

where $K\,(x+\Delta x/2)\approx\frac{1}{2}(K\,(x+\Delta x)+K\,(x))$ and $K\,(x-\Delta x/2)\approx\frac{1}{2}(K\,(x)+K\,(x-\Delta x))$. Thus,

$$\frac{\partial q}{\partial x}\approx -\frac{((K\,(x+\Delta x)+K\,(x))(\theta(x+\Delta x)-\theta(x))-(K\,(x)+K\,(x-\Delta x))(\theta(x)-\theta(x-\Delta x)))}{2(\Delta x)^2} \tag{58}$$

The same approximations are made for $\partial q/\partial y$ and $\partial q/\partial z$. These approximations are substituted into the energy equation to form the following iterative equation for each node in the mesh:

$$\theta(t+\Delta t)^K=\theta(t)+\Delta t\,\frac{(\phi\Lambda^{K-1}(t+\Delta t)+(1-\phi)\Lambda(t))}{\rho\beta C^{K-1}(t+\Delta t)+\rho(1-\beta)C(t)} \tag{59}$$

where $\Lambda(t)=\nabla\cdot K\cdot\nabla\theta(t)+(\rho z)(t)$ and $0\leqslant\beta\leqslant 1$. This iterative sequence is applied to each node in the mesh sequentially, for each node in the entire mesh, and then the values on the right-hand sides are updated, i.e $\theta^{K-1}(t+\Delta t)=\theta^K(t+\Delta t)$, and the procedure is repeated, $K=1,2,\ldots,$ until

$$\frac{\|\theta(t+\Delta t)^K-\theta(t+\Delta t)^{K-1}\|}{\|\theta(t+\Delta t)^K\|}\leqslant \text{tol} \tag{60}$$

If the iterations do not converge within a preset number of iterations, the time steps are reduced, and the procedure is repeated. In order to avoid 'chasing' alternating phase transformations (back and forth) within a time step, $\beta=0$. Any phase changes are recorded and used for the next time step.

5. STAGGERING SCHEMES FOR THERMO-ELECTROMAGNETICALLY COUPLED PROBLEMS

Staggering schemes typically proceed by solving each field equation individually, allowing only the primary field variable to be active. After the solution of each field equation, the primary field variable is updated, and the next field equation is addressed in a similar manner. Such approaches have a long history in the computational mechanics community. For example, see Park and Felippa [38], Felippa *et al.* [39], Zienkiewicz [40], Zienkiewicz *et al.* [41], Schrefler [42], Tursa and Schrefler [43], Lewis *et al.* [44], Doltsinis [45, 46], Piperno [47], Lewis and Schrefler [48], Armero and Simo [49–51], Armero [52], Le Tallec and Mouro [53], Zohdi [23–25] and the extensive works of Farhat and coworkers [54–58]. For a recent work involving staggering schemes for piezoelectric applications, see Fish and Chen [59]. In addition, for a review of the state of the art, see Michopoulos *et al.* [60]. Usually, if a recursive staggering process is *not employed* (an explicit coupling scheme), the staggering error can accumulate rapidly. However, an overkill approach (involving very small time steps, smaller than those needed to control the discretization error), simply to suppress a non-recursive staggering process error, is computationally inefficient. Therefore, the objective of the next subsection is to develop a strategy to adaptively adjust, in fact maximize, the choice of the time-step size in order to control the staggering error, while

DOI: 10.1002/nme

simultaneously staying below a critical time-step size needed to control the discretization error (as stated before). An important related issue is to simultaneously minimize the computational effort involved. The number of times the multifield system is solved, as opposed to time steps, is taken as the measure of computational effort since, within a time step, many multifield system re-solves can take place. We now further develop the staggering scheme introduced earlier by extending an approach found in Zohdi [23–25].

5.1. Abstract setting

We consider an abstract setting, whereby one solves for the nodal values for the electric field, assuming the magnetic and thermal fields are fixed,

$$\mathscr{A}_1(\underline{\mathbf{E}^{L+1,K}}, \mathbf{H}^{L+1,K-1}, \theta^{L+1,K-1}) = \mathscr{B}_1(\mathbf{E}^{L+1,K-1}, \mathbf{H}^{L+1,K-1}, \theta^{L+1,K-1}) \tag{61}$$

then one solves for the magnetic fields, assuming the nodal values fixed for the electric and thermal fields,

$$\mathscr{A}_2(\mathbf{E}^{L+1,K}, \underline{\mathbf{H}^{L+1,K}}, \theta^{L+1,K-1}) = \mathscr{B}_2(\mathbf{E}^{L+1,K}, \mathbf{H}^{L+1,K-1}, \theta^{L+1,K-1}) \tag{62}$$

then one solves for the thermal fields, assuming the nodal values fixed for the electric and magnetic fields,

$$\mathscr{A}_3(\mathbf{E}^{L+1,K}, \mathbf{H}^{L+1,K}, \underline{\theta^{L+1,K}}) = \mathscr{B}_3(\mathbf{E}^{L+1,K}, \mathbf{H}^{L+1,K}, \theta^{L+1,K-1}) \tag{63}$$

where the only underlined variable is 'active', L indicates the time step and K indicates the iteration counter. Within the staggering scheme, implicit time-stepping methods (with time-step size adaptivity) will be used throughout the upcoming analysis. We define the normalized errors within each time step, for the three fields,

$$\varpi_{E-K} \stackrel{\text{def}}{=} \frac{\|\mathbf{E}^{L+1,K} - \mathbf{E}^{L+1,K-1}\|}{\|\mathbf{E}^{L+1,K} - \mathbf{E}^{L}\|}, \quad \varpi_{H-K} \stackrel{\text{def}}{=} \frac{\|\mathbf{H}^{L+1,K} - \mathbf{H}^{L+1,K-1}\|}{\|\mathbf{H}^{L+1,K} - \mathbf{H}^{L}\|}$$
$$\varpi_{\theta-K} \stackrel{\text{def}}{=} \frac{\|\theta^{L+1,K} - \theta^{L+1,K-1}\|}{\|\theta^{L+1,K} - \theta^{L}\|} \tag{64}$$

Thereafter, we select the maximum error for adaptivity $\varpi_K^* \stackrel{\text{def}}{=} \max(\varpi_{E-K}, \varpi_{H-K}, \varpi_{\theta-K})$ and the scaling metric for adaptivity***

$$\Phi_K \stackrel{\text{def}}{=} \left(\frac{(C_{\text{tol}}/\varpi_0^*)^{1/pK_{\text{d}}}}{(\varpi_K^*/\varpi_0^*)^{1/pK}} \right) \tag{65}$$

5.2. Staggering algorithm

The algorithm is as follows ($\mathbf{W} = (\mathbf{E}, \mathbf{H}, \theta)$):

(1) Compute **E**-field with **H** and θ fixed, then compute **H**-field with **E** and θ fixed and then compute θ-field with **E** and **H** fixed.

(2) Compute error measures: $\varpi_K^* \stackrel{\text{def}}{=} \max(\varpi_{E-K}, \varpi_{H-K}, \varpi_{\theta-K})$.

***Clearly, $p = 1$, for a collection of first-order equations.

DOI: 10.1002/nme

(3) If tolerance is met, $\varpi^* \leqslant C_{\text{tol}}$ and $K \leqslant K_{\text{d}}$, then: (a) increment time forward: $t = t + \Delta t$, (b) construct new time step: $\Delta t = \Phi_K \Delta t$, where

$$\Phi_K \stackrel{\text{def}}{=} \left(\frac{(C_{\text{tol}}/\varpi_0^*)^{1/pK_{\text{d}}}}{(\varpi_K^*/\varpi_0^*)^{1/pK}} \right)$$

and (c) select $\Delta t = \min(\Delta t^{\text{lim}}, \Delta t)$ and go to (1).

(4) If tolerance is not met, $\varpi^* > C_{\text{tol}}$ and $K = K_{\text{d}}$, and then construct (refine) new time step: $\Delta t = \Phi_K \Delta t$ and go to (1).

The overall goal is to deliver solutions where the staggering (incomplete coupling) error is controlled and the temporal discretization accuracy dictates the upper limits on the time-step size (Δt^{lim}). Generally speaking, the staggering error, which is a function of the time-step size, is temporally variable and can become stronger, weaker or possibly oscillatory, is extremely difficult to ascertain *a priori* as a function of the time-step size. Therefore, to circumvent this problem, the adaptive strategy presented in this section was developed to provide accurate solutions by iteratively adjusting the time steps. Specifically, a sufficient condition for the convergence of the presented fixed-point scheme was that the spectral radius or contraction constant of the coupled operator, which depends on the time-step size, must be less than 1. This observation was used to adaptively maximize the time-step sizes, while simultaneously controlling the coupled operator's spectral radius, in order to deliver solutions below an error tolerance within a prespecified number of desired iterations. This recursive staggering error control can allow for substantial reduction in computational effort by the adaptive use of large time steps, where possible. Furthermore, such a recursive process has a reduced sensitivity, relative to an explicit staggering approach, to the order in which the individual equations are solved, since it is self-correcting.

5.3. Summary of solution schemes

In summary, clearly, there are various levels of solution methods that one can choose from (Figure 4):

- *Time stepping*: (a) implicit time stepping ($0 < \phi \leqslant 1$): (i) iterative or direct solution for electro-problem, (ii) iterative or direct solution for magneto-problem and (iii) iterative or direct solution for thermo-problem or (b) explicit time stepping ($\phi = 0$).
- *Overall field coupling*: (a) implicit staggering: (i) solve electro-problem, (ii) solve mageto-problem, (iii) solve thermo-problem, (iv) repeat cycle until convergence and (v) go to next time step or (b) explicit staggering: (i) solve electro-problem, (ii) solve mageto-problem, (iii) solve thermo-problem and (iv) go to next time step.

Remark

Clearly, one should use the previous (converged) time-step's solution as the starting guess for the next time step to obtain a 'head-start'. When selecting a time step, one must balance accuracy concerns[†††] and, simultaneously, stability issues. Clearly, the smaller the time step, the more stable the solution process; however, more time steps means more system evaluations. One would like to keep the time steps near the CFL limit or slightly below it. The CFL condition dictates that the numerical wave speed of $\Delta x/\Delta t$ must be at least as fast as the physical wave speed. In other words, $\Delta x/\Delta t \geqslant c$,

[†††] Typically, the number of iterations needed to solve the coupled system, if an iterative scheme is used, increases with the time-step size and the value of ϕ.

DOI: 10.1002/nme

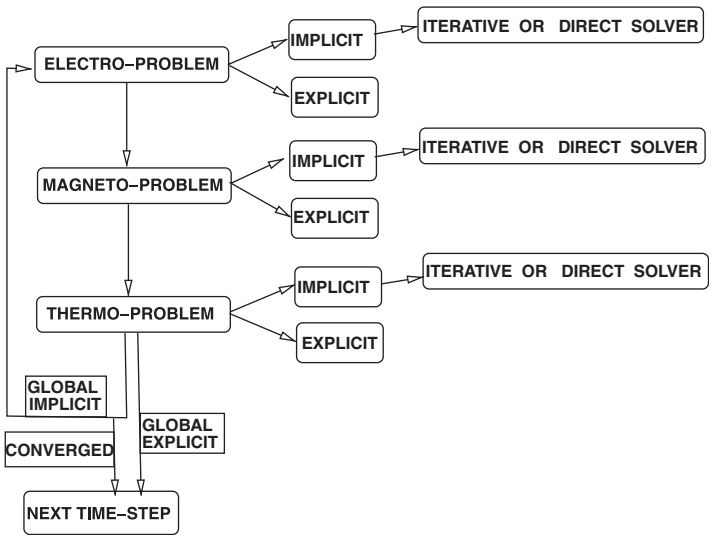

Figure 4. Levels of system solving.

which leads to the restriction $\Delta t \leqslant \Delta x/c$. Owing to the fact that we are dealing with heterogeneous media in three dimensions, an *ad hoc*, slightly conservative, restriction is

$$\Delta t \leqslant \frac{\min(\Delta x_1, \Delta x_2, \Delta x_3)}{c_{\max}} \tag{66}$$

where $c_{\max}$ is the fastest wave speed in the heterogeneous medium. Stability can, of course, be achieved by using an implicit scheme. However, in many cases, this critical condition (for explicit methods) still serves as an indicator of poor numerical behavior, *even for implicit schemes.* For the remainder of the study, we shall refer to the 'CFL number' as

$$\mathscr{C}\mathscr{F}\mathscr{L} \stackrel{\text{def}}{=} \Delta t \left(\frac{c_{\max}}{\min(\Delta x_1, \Delta x_2, \Delta x_3)} \right) \tag{67}$$

6. A MODEL PROBLEM

We consider an example of a heterogeneous material combination composed of a group of particles in a binding matrix. All tests were run on an ordinary laptop; therefore, such simulations are easily reproducible elsewhere for other parameter selections. As an example, we considered a group of N_p randomly dispersed spherical particles, of equal size, in a cubical domain of dimensions $D \times D \times D$. The particle size and volume fraction were determined by a particle/sample size ratio, which was defined via a subvolume size $V \stackrel{\text{def}}{=} D \times D \times D/N_p$. The non-dimensional ratio of the radius (b) to the subvolume was denoted by $\mathscr{L} \stackrel{\text{def}}{=} b/V^{1/3}$. The volume fraction occupied by the particles can be consequently expressed as $v_p \stackrel{\text{def}}{=} 4\pi\mathscr{L}^3/3$. Thus, the total volume occupied by the particles denoted by ζ can be expressed as $\zeta = v_p N_p V$. We used $N_p = 100$ particles (Figure 5).

DOI: 10.1002/nme

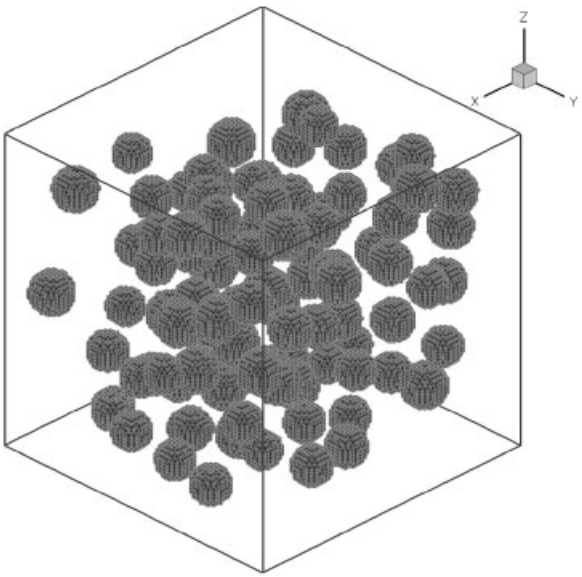

Figure 5. The morphology of the test sample's numerically resolved microstructure.

This sample size was successively enlarged until there were no significant changes in the overall system response for further enlargements.[‡‡‡]

The classical random sequential addition algorithm was used to place non-overlapping particles randomly into the domain of interest (RSA, [62]). This algorithm was adequate for the volume fraction range of interest. However, if higher volume fractions are desired, more sophisticated algorithms, such as the well-known, equilibrium-based, Metropolis algorithm can be used. For even higher volume fractions, effectively packing (and 'jamming') particles, a relatively new class of efficient methods, based on simultaneous particle flow and growth, has been developed by Torquato and coworkers [16, 63–66].

6.1. System parameters

The speed of electromagnetic wave propagation is $c=1/\sqrt{\varepsilon_0\mu_0}\approx 2.997924562\times 10^8\pm 1.1\,\mathrm{m/s}$ in a vacuum. The free space electric permittivity is $\varepsilon_0=1/c^2\mu_0=8.8542\times 10^{-12}\,\mathrm{C^2/N/m^2}$ and the free space magnetic permeability is $\mu_0=4\pi\times 10^{-7}\,\mathrm{Wb/A/m}=1.2566\times 10^{-6}\,\mathrm{Wb/A/m}$. Usually, for electromagnetic materials, we express $\varepsilon=\varepsilon_0\varepsilon_r$, where $\varepsilon_0=8.854\times 10^{-12}$ F/m is the free space permittivity, ε_r is the relative permittivity or 'dielectric' constant, and $\mu_0=4\pi\times 10^{-7}\,\mathrm{N\,s^2/C^2}$ and $\mu=\mu_r\mu_0$, where μ_r is the relative magnetic permeability. The following parameters were used: number of nodes used, $30\times 30\times 30$; (inner loop) solver tolerance, $\mathrm{tol}=10^{-6}$; size of the sample, $D\times D\times D$, with a subsample having a length scale of $0.80\times D$, $D=0.00005$ m; electric field on the boundary (linearly growing), $\mathbf{E}=(0,10^9,0)10t/T$, initial conditions, $\mathbf{E}=(0,0,0)$; magnetic field on the boundary (linearly growing), $\mathbf{H}=(0,0,10^9)\sqrt{\mu_0/\varepsilon_0}10t/T$, initial conditions, $\mathbf{H}=(0,0,0)$;

[‡‡‡]For a more in-depth discussion on size-effect issues, see the works of Zohdi and collaborators [21, 23–34, 61].

DOI: 10.1002/nme

time-stepping factor, $\phi = 0.5$ (mid-point rule); temperature on the boundary, $\theta = 303.13\,\mathrm{K}$; initial conditions, $\theta = 303.13\,\mathrm{K}$; the relative permittivity of the particles, $\varepsilon_{2r} = 4$; the relative permittivity of the matrix, $\varepsilon_{1r} = 1$; the relative permeability of the particles, $\mu_{2r} = 2$; the relative permeability of the matrix, $\mu_{1r} = 1$; the electrical conductivity of the particles $\sigma_2 = 1$; the electrical conductivity of the matrix $\sigma_1 = 1$; the density of the particles, $\rho_2 = 2000$; the density of the matrix, $\rho_1 = 1000$; the thermal conductivity of the particles, $K_2 = 200$; the thermal conductivity of the matrix, $K_1 = 100$; the heat capacity of the particles, $C_2 = 2000$, $C_{2m} = 2000$; the heat capacity of the matrix, $C_1 = 1000$, $C_{1m} = 1500$; the absorbtivity of the particles, $a_2 = 0.5$; the absorbtivity of the matrix, $a_1 = 0.5$; $\Delta H_{2m}^{\mathrm{S}\to\mathrm{L}} = 2000$; $\Delta H_{1m}^{\mathrm{S}\to\mathrm{L}} = 1000$; $\Delta\theta_{2m} = 1$; $\Delta\theta_{1m} = 1$; $\mathscr{L} = 0.375$; $\theta_{2m} = 500$; $\theta_{1m} = 1000$; $K_{\varepsilon_1} = 0.01$; $K_{\mu_1} = 0.01$; $K_{\varepsilon_2} = 0.01$; $K_{\mu_2} = 0.01$; $\theta_0 = 303.13$; the number of desired iterations per time step was set to $K_{\mathrm{d}} = 5$; and the coupling tolerance was set to $C_{\mathrm{tol}} = 10^{-6}$.

6.2. Results

The meshes were repeatedly refined in the following manner:

- A $41 \times 41 \times 41$ mesh, which has 413 526 *electromagnetic degrees of freedom* and 68 921*thermodynamic degrees of freedom* for a total of 482 447 *degrees of freedom*.
- A $61 \times 61 \times 61$ mesh, which has 1 361 886 *electromagnetic degrees of freedom* and 226 981 *thermodynamic degrees of freedom* for a total of 1 588 867 *degrees of freedom*.
- A $81 \times 81 \times 81$ mesh, which has 3 188 646 *electromagnetic degrees of freedom* and 531 441 *thermodynamic degrees of freedom* for a total of 3 720 087 *degrees of freedom*.
- A $101 \times 101 \times 101$ mesh, which has 6 181 806 *electromagnetic degrees of freedom* and 1 030 301 *thermodynamic degrees of freedom* for a total of 7 212 107 *degrees of freedom*.

Approximately beyond the 61/81-level there were no perceivable changes in the results. We have the following observations:

- At the length scales of interest, it is questionable whether the ideas of a sharp material interface are sensible. Accordingly, we simulated the system with and without (classical) Laplacian smoothing, whereby one smooths the material data by post-processing the material data by enforcing

$$\nabla^2 \boldsymbol{\mu} = \mathbf{0} \tag{68}$$

  This was done node by node by computing a new material representation via

$$\hat{\boldsymbol{\mu}}_{i,j,k} = \tfrac{1}{6}(\boldsymbol{\mu}_{i+1,j,k} + \boldsymbol{\mu}_{i-1,j,k} + \boldsymbol{\mu}_{i,j+1,k} + \boldsymbol{\mu}_{i,j-1,k} + \boldsymbol{\mu}_{i,j,k+1} + \boldsymbol{\mu}_{i,j,k-1}) \tag{69}$$

  The same was done for the permittivity by enforcing $\nabla^2 \boldsymbol{\varepsilon} = \mathbf{0}$, as well as other material data. The simulations were run with and without smoothed data, with the results being negligibly different for sufficiently fine meshes (Figure 5).
- The effective electric flux increases more for the thermally sensitive material than for the thermally insensitive material.
- The effective electric field initially increases more for the thermally sensitive material; however, it decreases with increasing time. The effect can be qualitatively explained by

DOI: 10.1002/nme

realizing that[§§§]

$$\nabla \times \mathbf{H} = \frac{\partial(\varepsilon \mathbf{E})}{\partial t} \;\Rightarrow\; \mathbf{E} = \underbrace{\frac{1}{\partial \varepsilon / \partial t}}_{\gg 0} \left(\nabla \times \mathbf{H} - \varepsilon \frac{\partial \mathbf{E}}{\partial t} \right) \tag{70}$$

The same trend holds for the magnetic field

$$-\nabla \times \mathbf{E} = \frac{\partial(\mu \mathbf{H})}{\partial t} \;\Rightarrow\; \mathbf{H} = -\underbrace{\frac{1}{\partial \mu / \partial t}}_{\gg 0} \left(\nabla \times \mathbf{E} + \mu \frac{\partial \mathbf{H}}{\partial t} \right) \tag{71}$$

- Note that the time steps were initially set to be the CFL limit $\mathscr{C}\mathscr{F}\mathscr{L} \stackrel{\text{def}}{=} \Delta t (c_{\max} / \min(\Delta x_1, \Delta x_2, \Delta x_3)) = 1$, but had to be refined below that level for the thermally sensitive case. The coupling tolerance was set to $C_{\text{tol}} = 10^{-6}$ in the preceding calculations. Both the thermally insensitive and thermally sensitive problems required time-step adaptivity to control the coupling error, although the time-step sizes needed for the thermally sensitive problem were smaller than those for the thermally insensitive problem. However, if the C_{tol} was made coarser, for example, to $C_{\text{tol}} = 10^{-5}$ and $C_{\text{tol}} = 10^{-4}$, etc., eventually the CFL-time step was adequate for the thermally insensitive problem. Clearly, these results are dependent on the material parameter selected. However, an important point which we emphasize is that it is virtually impossible to determine *a priori* whether the initial time step is adequate to meet a tolerance and whether adaptivity is needed (Figures 6–13).

7. COMPARISON OF THE NUMERICAL AND ANALYTICAL RESPONSES (BOUNDS)

The preceding results are quite important from both a theoretical and computational point of view. Until recently, the direct computation of micromaterial responses was very difficult. Analytical bounds provide some 'assurance' that the computed responses are realistic. The numerical responses were checked against the following analytical bounds:

- The Hill–Reuss–Voigt–Wiener bounds (for the case of isotropic materials):

$$\left(\frac{v_p}{\varepsilon_p} + \frac{1 - v_p}{\varepsilon_m} \right)^{-1} = \langle \varepsilon^{-1}(\mathbf{x}) \rangle_\Omega^{-1} \leqslant \varepsilon^* \leqslant \langle \varepsilon(\mathbf{x}) \rangle_\Omega = v_p \varepsilon_p + (1 - v_p) \varepsilon_m \tag{72}$$

where v_p is the volume fraction of the particles, ε_p is the permittivity of the particles, ε_m is the permittivity of the matrix and

$$\left(\frac{v_p}{\mu_p} + \frac{1 - v_p}{\mu_m} \right)^{-1} = \langle \mu^{-1}(\mathbf{x}) \rangle_\Omega^{-1} \leqslant \mu^* \leqslant \langle \mu(\mathbf{x}) \rangle_\Omega = v_p \mu_p + (1 - v_p) \mu_m \tag{73}$$

where μ_p is the permeability of the particles and μ_m is the permeability of the matrix.

[§§§] For simplicity of explanation, we ignore the loss terms.

DOI: 10.1002/nme

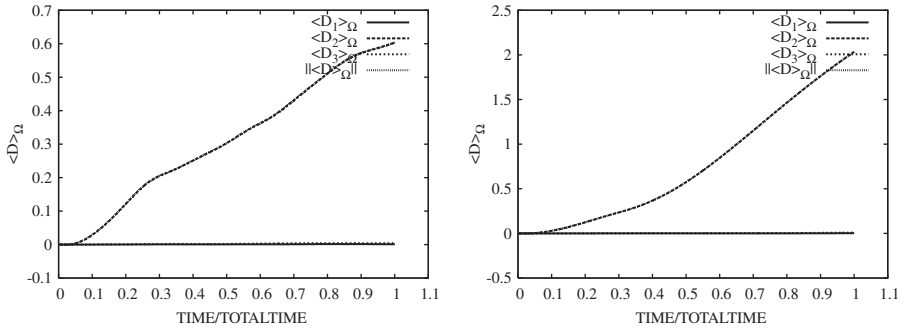

Figure 6. The effective electric flux ($\langle \mathbf{D} \rangle_\Omega$). Left: thermally insensitive case and right: thermally sensitive case.

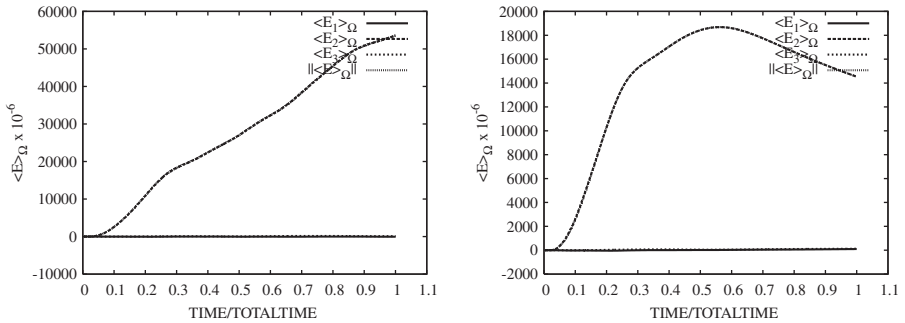

Figure 7. The effective electric field ($\langle \mathbf{E} \rangle_\Omega$). Left: thermally insensitive case and right: thermally sensitive case.

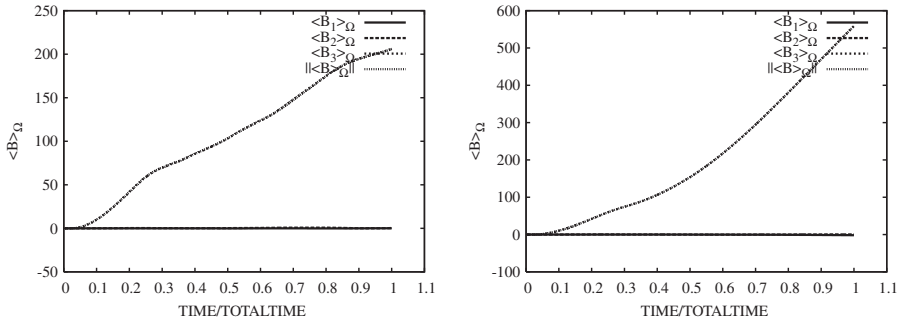

Figure 8. The effective magnetic flux ($\langle \mathbf{B} \rangle_\Omega$). Left: thermally insensitive case and right: thermally sensitive case.

DOI: 10.1002/nme

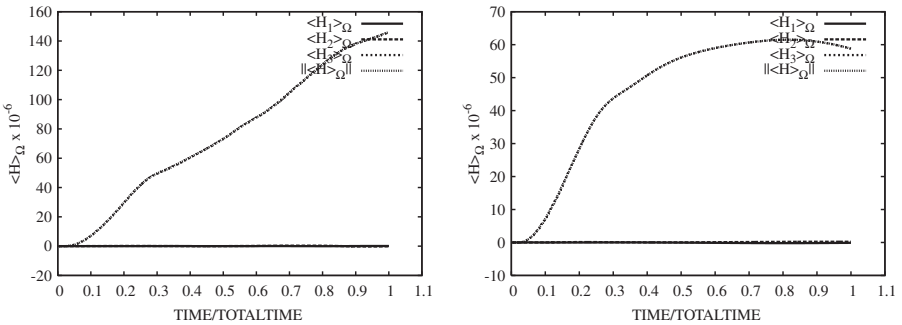

Figure 9. The effective magnetic field ($\langle \mathbf{H} \rangle_\Omega$). Left: thermally insensitive case and right: thermally sensitive case.

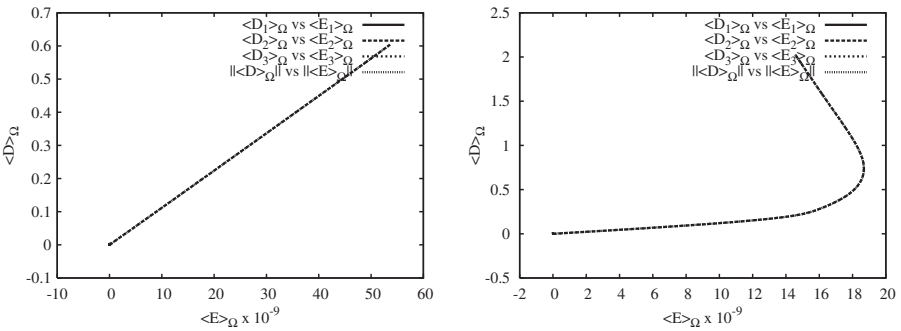

Figure 10. The effective permittivity ($\boldsymbol{\varepsilon}^*$). Left: thermally insensitive case and right: thermally sensitive case.

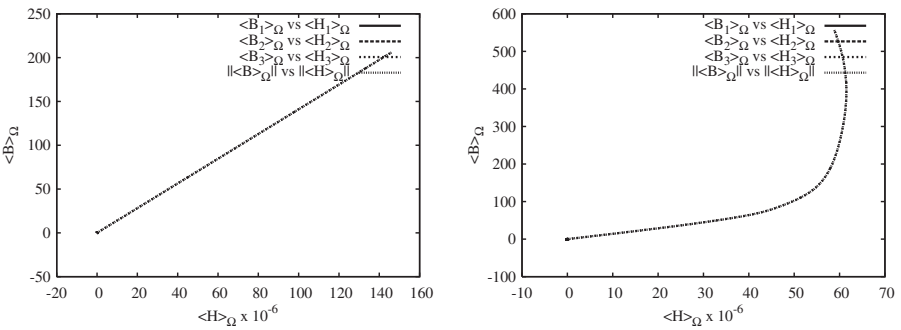

Figure 11. The effective permeability ($\boldsymbol{\mu}^*$). Left: thermally insensitive case and right: thermally sensitive case.

DOI: 10.1002/nme

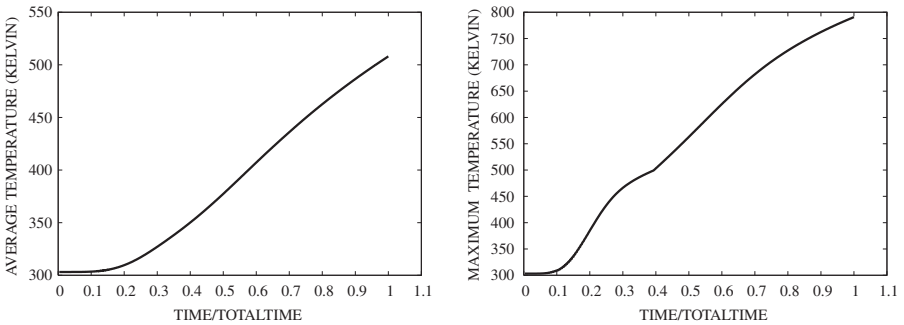

Figure 12. Left: average temperature ($\langle\theta\rangle_\Omega$) and right: the maximum temperature, for the thermally sensitive case.

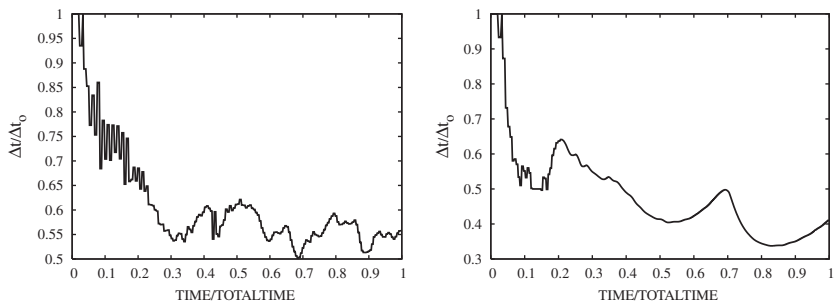

Figure 13. Time-step size relative to the $\mathscr{CFL}$-limit size (constant for the uncoupled problem). Left: thermally insensitive case and right: thermally sensitive case. The time steps were initially set to be the CFL limit $\mathscr{CFL} \stackrel{\text{def}}{=} \Delta t\,(c_{\max}/\min(\Delta x_1, \Delta x_2, \Delta x_3)) = 1$, but had to be refined below that level.

- The Hashin–Shtrikman bounds

$$\langle \varepsilon^{-1}(\mathbf{x})\rangle_\Omega^{-1} \leqslant \varepsilon_1 + \underbrace{\frac{v_2^\varepsilon}{\dfrac{1}{\varepsilon_2-\varepsilon_1}+\dfrac{1-v_2^\varepsilon}{3\varepsilon_1}}}_{\varepsilon^{*,-}} \leqslant \varepsilon^* \leqslant \varepsilon_2 + \underbrace{\frac{1-v_2^\varepsilon}{\dfrac{1}{\varepsilon_1-\varepsilon_2}+\dfrac{v_2^\varepsilon}{3\varepsilon_2}}}_{\varepsilon^{*,+}} \leqslant \langle \varepsilon(\mathbf{x})\rangle_\Omega \tag{74}$$

and the overall permeability

$$\langle \mu^{-1}(\mathbf{x})\rangle_\Omega^{-1} \leqslant \mu_1 + \underbrace{\frac{v_2^\mu}{\dfrac{1}{\mu_2-\mu_1}+\dfrac{1-v_2^\mu}{3\mu_1}}}_{\mu^{*,-}} \leqslant \mu^* \leqslant \mu_2 + \underbrace{\frac{1-v_2^\mu}{\dfrac{1}{\mu_1-\mu_2}+\dfrac{v_2^\mu}{3\mu_2}}}_{\mu^{*,+}} \leqslant \langle \mu(\mathbf{x})\rangle_\Omega \tag{75}$$

where $\varepsilon_2 \geqslant \varepsilon_1$, $\mu_2 \geqslant \mu_1$, v_2^ε is the volume fraction of the phase with the higher ε value ('phase 2' in the former expression) for the permittivity mismatch and v_2^μ is the volume fraction of the phase with the higher μ value ('phase 2' in the latter expression) for the permeability

DOI: 10.1002/nme

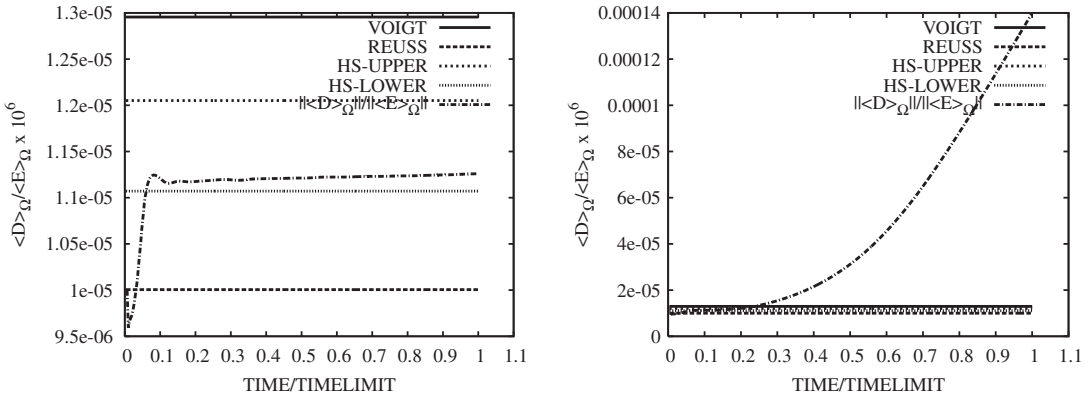

Figure 14. The effective permittivity ($\boldsymbol{\varepsilon}^*$). Left: thermally insensitive result and right: thermally sensitive result.

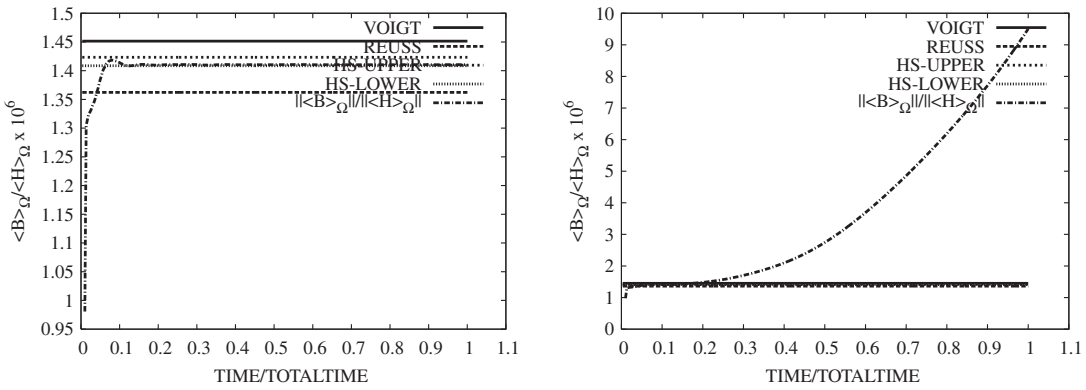

Figure 15. The effective permeability ($\boldsymbol{\mu}^*$). Left: thermally insensitive result and right: thermally sensitive result.

mismatch.[¶¶¶] Such bounds are the tightest known on isotropic effective responses, with isotropic two-phase microstructures, where only the volume fractions and phase contrasts of the constituents are known. Note that no further geometric information, such as the number and nature of particles, etc., contributes to these bounds.

For both thermally sensitive and insensitive cases, both the effective permeability and the permittivity increase to match the lower Hashin–Shtrikman bounds. However, in the case of the thermally sensitive results, they eventually exceed the bounds due to the pointwise increase in the material values due to thermal effects (Figures 14 and 15).

[¶¶¶]For either case, the volume fraction of the other phase is v_1, where $v_1 + v_2 = 1$.

DOI: 10.1002/nme

8. CONCLUDING REMARKS: INVERSE PROBLEMS

An important aspect of any model is the identification of parameters which force the system behavior to match a (desired) target response. For example, in the ideal case, one would like to determine the type of microstructural parameters that produce certain effective responses, via numerical simulations, in order to guide or minimize the time-consuming laboratory tests. A relatively straightforward way of achieving this is to consider inverse problems whereby particulate parameters are sought which deliver a desired overall behavior by minimizing a cost. An obvious example of an objective function that one might minimize is

$$\Pi = w_1 \left(\frac{\|\boldsymbol{\varepsilon}^* - \boldsymbol{\varepsilon}^{*,\mathrm{D}}\|}{\|\boldsymbol{\varepsilon}^{*,\mathrm{D}}\|} \right)^2 + w_2 \left(\frac{\|\boldsymbol{\mu}^* - \boldsymbol{\mu}^{*,\mathrm{D}}\|}{\|\boldsymbol{\mu}^{*,\mathrm{D}}\|} \right)^2 + \text{thermal constraints} \tag{76}$$

where $\boldsymbol{\varepsilon}^{*,\mathrm{D}}$ and $\boldsymbol{\mu}^{*,\mathrm{D}}$ are the desired overall properties and w_1 and w_2 are the design weights that indicate the importance of achieving each component of the objective. Specifically, a microstructural design problem can be set up by defining an N-tuple design vector, denoted as $\Lambda \overset{\text{def}}{=} (\Lambda_1, \Lambda_2, \ldots, \Lambda_N)$, for example, consisting of the following components: (1) the properties of the particles, (2) the volume fraction of the particles and (3) the topology of the particles. Ellipsoidal shapes are qualitatively useful since the geometry can closely represent a variety of particulate types, for example, platelets when the ellipsoids are oblate or needles (discontinuous fibers) when the ellipsoids are prolate. Such shapes can be generalized by considering the following equation (Figure 16):

$$\left(\frac{|x - x_0|}{r_1} \right)^{s_1} + \left(\frac{|y - y_0|}{r_2} \right)^{s_2} + \left(\frac{|z - z_0|}{r_3} \right)^{s_3} = 1 \tag{77}$$

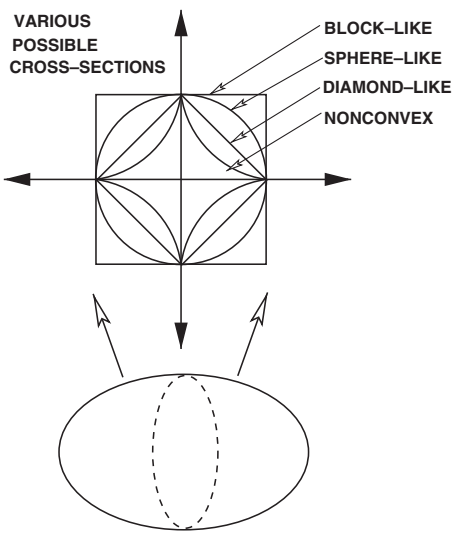

Figure 16. A generalized (particle) ellipsoid.

DOI: 10.1002/nme

where the s's are exponents. Values of $s<1$ produce non-convex shapes, whereas $s>2$ values produce 'block-like' shapes. The following are free system variables: (1) *Particulate properties*: for example, assuming local isotropy of the particles, ε_2 and μ_2 (two variables), (2) *Particulate topology*: for example, the polynomial order of generalized ellipsoids, s (three variables), (3) *Particulate aspect ratio*: for example, defined by $\mathrm{AR} \stackrel{\mathrm{def}}{=} r_1/r_2 = r_1/r_3$, where $r_2 = r_3$, $\mathrm{AR}>1$ for prolate geometries and $\mathrm{AR}<1$ for oblate shapes (one variable), (4) *Particulate volume fraction*: for example, v_2 (one variable), (5) *Particulate orientation*: for example, within the last decade there have been viable processing methods developed to control the orientation of particulate matter by coating them with a conducting liquid material, introducing them into the molten matrix material (three free variables, i.e. Euler angles: α_1, α_2, α_3), and applying an electrical current to force the particles to align themselves along the field lines (see, Michaud [67]). This will produce overall anisotropic properties and (6) *Matrix properties*: for example, if the matrix material is free to change, assuming local isotropy of the matrix material, ε_1 and μ_1 (two variables). We remark that if the particles' orientations are assumed to be aligned, then three more (angular orientation) parameters can be introduced $(\alpha_1, \alpha_2, \alpha_3)$. In fact, suspensions can become aligned, for example, along electrical field lines induced by external sources or due to flow conditions. Thus, the search space grows to more parameters, $\Lambda = (\varepsilon_1, \mu_1, \varepsilon_2, \mu_2, v_2, s_1, s_2, s_3, \mathrm{AR}, \alpha_1, \alpha_2, \alpha_3, \text{etc.})$. Generally, Π will depend on the design variables in a non-convex and non-differentiable manner (especially if there are constraints) on the microstructural parameters. The minimization of Π can be achieved by using 'genetic' algorithms (GA), before applying classical gradient-based schemes.[IIIII] GA are search methods based on the principles of natural selection, drawing upon concepts of species evolution, such as reproduction, mutation and crossover. Implementation typically involves a randomly generated population of 'genetic' strings, each of which represents a specific choice of system parameters. The population of genes undergo 'mating sequences', 'offspring production' and other biologically inspired events in order to find regions of the search space where cost functions are small. These methods have a long history, dating back, at least, to the seminal work of Holland [71]. For reviews, see Goldberg [72], Davis [73], Onwubiko [74], Kennedy and Eberhart [75], Lagaros *et al.* [76], Papadrakakis *et al.* [77–80] and Goldberg and Deb [81]. In Zohdi [21, 24–34], GA have been developed to treat a wide variety of inverse problems involving various aspects of multiparticle systems, and we refer the interested reader to those works.

REFERENCES

1. Maxwell JC. On the dynamical theory of gases. *Philosophical Transactions of the Royal Society of London* 1867; **157**:49.
2. Maxwell JC. *A Treatise on Electricity and Magnetism* (3rd edn). Clarendon Press: Oxford, 1873.
3. Rayleigh JW. On the influence of obstacles arranged in rectangular order upon properties of a medium. *Philosophical Magazine* 1892; **32**:481–491.
4. Voigt W. Über die Beziehung zwischen den beiden Elastizitätskonstanten isotroper Körper. *Wiedemanns Annalen* 1889; **38**:573–587.
5. Reuss A. Berechnung der Fliessgrenze von Mischkristallen auf Grund der Plastizitätsbedingung für Einkristalle. *Zeitschrift für Angewandte Mathematik und Mechanik* 1929; **9**:49–58.
6. Hill R. The elastic behaviour of a crystalline aggregate. *Proceedings of the Physical Society of London* 1952; **A65**:349–354.

[IIIII] An exhaustive review of these methods can be found in the texts of Luenberger [68] and Gill *et al.* [69], while a state of the art can be found in Papadrakakis *et al.* [70].

DOI: 10.1002/nme

7. Wiener O. Zur Theorie der Refraktionskonstanten. *Berichte über die Verhandlungen der Königlich-Sächsischen Gesellschaft der Wissenshaften zu Leipzig*. Mathematik–Physik Klasses, vol. 62, 1910; 256–277.
8. Hashin Z, Shtrikman S. On some variational principles in anisotropic and nonhomogeneous elasticity. *Journal of the Mechanics and Physics of Solids* 1962; **10**:335–342.
9. Hashin Z, Shtrikman S. A variational approach to the theory of the elastic behaviour of multiphase materials. *Journal of the Mechanics and Physics of Solids* 1963; **11**:127–140.
10. Hashin Z, Shtrikman S. A variational approach to the theory of effective magnetic permeability of multiphase materials. *Journal of Applied Physics* 1962; **33**(10):3125–3131.
11. Hashin Z. Analysis of composite materials: a survey. *Journal of Applied Mechanics* (ASME) 1983; **50**:481–505.
12. Torquato S. Random heterogeneous media: microstructure and improved bounds on effective properties. *Applied Mechanics Reviews* 1991; **44**:37–76.
13. Torquato S, Lado F. Improved bounds on the effective elastic moduli of random arrays of cylinders. *Journal of Applied Mechanics* 1992; **59**:1–6.
14. Torquato S. Effective stiffness tensor of composite media. I. Exact series expansions. *Journal of the Mechanics and Physics of Solids* 1997; **45**:1421–1448.
15. Torquato S. Effective stiffness tensor of composite media. II. Applications to isotropic dispersions. *Journal of the Mechanics and Physics of Solids* 1998; **46**:1411–1440.
16. Torquato S. *Random Heterogeneous Materials*: *Microstructure and Macroscopic Properties*. Springer: New York, 2002.
17. Jikov VV, Kozlov SM, Olenik OA. *Homogenization of Differential Operators and Integral Functionals*. Springer: Berlin, 1994.
18. Aboudi J. *Mechanics of Composite Materials—A Unified Micromechanical Approach*. Elsevier: Amsterdam, 1992; 29.
19. Mura T. *Micromechanics of Defects in Solids* (2nd edn). Kluwer Academic Publishers: Dordrecht, 1993.
20. Nemat-Nasser S, Hori M. *Micromechanics*: *Overall Properties of Heterogeneous Solids* (2nd edn). Elsevier: Amsterdam, 1999.
21. Zohdi TI, Wriggers P. *Introduction to Computational Micromechanics*. Springer: Berlin, 2005.
22. Kröner E. *Statistical Continuum Mechanics*. CISM Lecture Notes, vol. 92. Springer: Berlin, 1972.
23. Zohdi TI. An adaptive-recursive staggering strategy for simulating multifield coupled processes in microheterogeneous solids. *International Journal for Numerical Methods in Engineering* 2002; **53**:1511–1532.
24. Zohdi TI. Computational design of swarms. *International Journal for Numerical Methods in Engineering* 2003; **57**:2205–2219.
25. Zohdi TI. Genetic optimization of statistically uncertain microheterogeneous solids. *Philosophical Transactions of the Royal Society A*: *Mathematical*, *Physical and Engineering Sciences* 2003; **361**(1806):1021–1043.
26. Zohdi TI. On the compaction of cohesive hyperelastic granules at finite strains. *Proceedings of the Royal Society A*: *Mathematical*, *Physical and Engineering Sciences* 2003; **454**(2034):1395–1401.
27. Zohdi TI. Modeling and simulation of a class of coupled thermo-chemo-mechanical processes in multiphase solids. *Computer Methods in Applied Mechanics and Engineering* 2004; **193**(6–8):679–699.
28. Zohdi TI. Modeling and direct simulation of near-field granular flows. *International Journal of Solids and Structures* 2004; **42**(2):539–564.
29. Zohdi TI. A computational framework for agglomeration in thermo-chemically reacting granular flows. *Proceedings of the Royal Society of London*, *Series A* 2004; **460**:3421–3445.
30. Zohdi TI. Charge-induced clustering in multifield particulate flow. *International Journal for Numerical Methods in Engineering* 2005; **62**(7):870–898.
31. Zohdi TI. Computation of the coupled thermo-optical scattering properties of random particulate systems. *Computer Methods in Applied Mechanics and Engineering* 2006. Available from: http://www.sciencedirect.com/science/journal/00457825.
32. Zohdi TI. On the optical thickness of disordered particulate media. *Mechanics of Materials* 2006; **38**:969–981.
33. Zohdi TI, Kuypers FA. Modeling and rapid simulation of multiple red blood cell light scattering. *Journal of the Royal Society Interface* 2006; **3**(11):823–831.
34. Zohdi TI. *Introduction to the Modeling and Simulation of Particulate Flows*. SIAM: Philadelphia, PA, 2007.
35. Yee K. Numerical solution of initial boundary value problems involving Maxwell's equations in isotropic media. *IEEE Transactions on Antennas and Propagation* 1966; **14**:302.
36. Kunz KS, Luebbers RJ. *The Finite Difference Time Domain Method for Electromagnetics*. CRC Press: Boca Raton, FL, 1993.

DOI: 10.1002/nme

37. Taflove A, Hagness S. *Computational Electrodynamics*: *The Finite-difference Time-domain Method* (3rd edn). Artech Press: 2005.
38. Park KC, Felippa CA. Partitioned analysis of coupled systems. In *Computational Methods for Transient Analysis*, Belytschko T, Hughes TJR (eds), 1983.
39. Felippa CA, Park KC, Farhat C. Partitioned analysis of coupled mechanical systems. *Computer Methods in Applied Mechanics and Engineering* 2001; **190**:3247–3270.
40. Zienkiewicz OC. Coupled problems and their numerical solution. In *Numerical Methods in Coupled Systems*, Lewis RW, Bettes P, Hinton E (eds). Wiley: Chichester, 1984; 35–58.
41. Zienkiewicz OC, Paul DK, Chan AHC. Unconditionally stable staggered solution procedure for soil–pore fluid interaction problems. *International Journal for Numerical Methods in Engineering* 1988; **26**:1039–1055.
42. Schrefler BA. A partitioned solution procedure for geothermal reservoir analysis. *Communications in Applied Numerical Methods* 1985; **1**:53–56.
43. Tursa E, Schrefler BA. On consistency, stability and convergence of staggered solution procedures. *Rend. Mat. acc. Lincei*, *Rome*, *S. 9* 1994; **5**:265–271.
44. Lewis RW, Schrefler BA, Simoni L. Coupling versus uncoupling in soil consolidation. *International Journal for Numerical and Analytical Methods in Geomechanics* 1992; **15**:533–548.
45. Doltsinis I St. Coupled field problems–solution techniques for sequential and parallel processing. In *Solving Large–scale Problems in Mechanics*, Papadrakakis MM (ed.), 1993.
46. Doltsinis I St. Solution of coupled systems by distinct operators. *Engineering Computations* 1997; **14**:829–868.
47. Piperno S. Explicit/implicit fluid/structure staggered procedures with a structural predictor and fluid subcycling for 2D inviscid aeroelastic simulations. *International Journal for Numerical Methods in Fluids* 1997; **25**:1207–1226.
48. Lewis RW, Schrefler BA. *The Finite Element Method in the Static and Dynamic Deformation and Consolidation of Porous Media* (2nd edn). Wiley: New York, 1998.
49. Armero F, Simo JC. A new unconditionally stable fractional step method for non-linear coupled thermomechanical problems. *International Journal for Numerical Methods in Engineering* 1992; **35**:737–766.
50. Armero F, Simo JC. A-priori stability estimates and unconditionally stable product formula algorithms for non-linear coupled thermoplasticity. *International Journal of Plasticity* 1993; **9**:149–182.
51. Armero F, Simo JC. Formulation of a new class of fractional-step methods for the incompressible MHD equations that retains the long-term dissipativity of the continuum dynamical system. *Integration Algorithms for Classical Mechanics*. The Fields Institute Communications, vol. 10, 1996; 1–23.
52. Armero F. Formulation and finite element implementation of a multiplicative model of coupled poro-plasticity at finite strains under fully saturated conditions. *Computer Methods in Applied Mechanics and Engineering* 1999; **171**:205–241.
53. Le Tallec P, Mouro J. Fluid–structure interaction with large structural displacements. *Computer Methods in Applied Mechanics and Engineering* 2001; **190**(24–25):3039–3067.
54. Piperno S, Farhat C, Larrouturou B. Partitioned procedures for the transient solution of coupled aeroelastic problems—Part I: model problem, theory, and two-dimensional application. *Computer Methods in Applied Mechanics and Engineering* 1995; **124**(1–2):79–112.
55. Farhat C, Lesoinne M, Maman N. Mixed explicit/implicit time integration of coupled aeroelastic problems: three-field formulation, geometric conservation and distributed solution. *International Journal for Numerical Methods in Fluids* 1995; **21**:807–835.
56. Lesoinne M, Farhat C. Free staggered algorithm for nonlinear transient aeroelastic problems. *AIAA Journal* 1998; **36**(9):1754–1756.
57. Farhat C, Lesoinne M. Two efficient staggered procedures for the serial and parallel solution of three-dimensional nonlinear transient aeroelastic problems. *Computer Methods in Applied Mechanics and Engineering* 2000; **182**:499–516.
58. Farhat C, van der Zee G, Geuzaine P. Provably second-order time-accurate loosely-coupled solution algorithms for transient nonlinear computational aeroelasticity. *Computer Methods in Applied Mechanics and Engineering* 2006; **195**:1973–2001.
59. Fish J, Chen W. Modeling and simulation of piezocomposites. *Computer Methods in Applied Mechanics and Engineering* 2003; **192**:3211–3232.
60. Michopoulos G, Farhat C, Fish J. Survey on modeling and simulation of multiphysics systems. *Journal of Computing and Information Science in Engineering* 2005; **5**(3):198–213.
61. Zohdi TI, Wriggers P. Aspects of the computational testing of the mechanical properties of microheterogeneous material samples. *International Journal for Numerical Methods in Engineering* 2001; **50**:2573–2599.

DOI: 10.1002/nme

62. Widom B. Random sequential addition of hard spheres to a volume. *Journal of Chemical Physics* 1966; **44**:3888–3894.
63. Kansaal A, Torquato S, Stillinger F. Diversity of order and densities in jammed hard-particle packings. *Physical Review E* 2002; **66**:041109.
64. Donev A, Cisse I, Sachs D, Variano EA, Stillinger F, Connelly R, Torquato S, Chaikin P. Improving the density of jammed disordered packings using ellipsoids. *Science* 2004; **13**(303):990–993.
65. Donev A, Torquato S, Stillinger F. Neighbor list collision-driven molecular dynamics simulation for nonspherical hard particles—I. Algorithmic details. *Journal of Computational Physics* 2005; **202**:737.
66. Donev A, Torquato S, Stillinger F. Neighbor list collision-driven molecular dynamics simulation for nonspherical hard particles—II. Application to ellipses and ellipsoids. *Journal of Computational Physics* 2005; **202**:765.
67. Michaud V. Liquid state processing. In *Fundamentals of Metal Matrix Composites*, Suresh S, Mortensen A, Needleman A (eds), 1992.
68. Luenberger D. *Introduction to Linear and Nonlinear Programming*. Addison-Wesley: Menlo Park, 1974.
69. Gill P, Murray W, Wright M. *Practical Optimization*. Academic Press: New York, 1995.
70. Papadrakakis M, Lagaros N, Tsompanakis Y, Plevris V. Large scale structural optimization: computational methods and optimization algorithms. *Archives of Computational Methods in Engineering*, *State of the Art Reviews* 2001; **8**(3):239–301.
71. Holland JH. *Adaptation in Natural and Artificial Systems*. University of Michigan Press: Ann Arbor, MI, 1975.
72. Goldberg DE. *Genetic Algorithms in Search*, *Optimization and Machine Learning*. Addison-Wesley: Reading, MA, 1989.
73. Davis L. *Handbook of Genetic Algorithms*. Thompson Computer Press: 1991.
74. Onwubiko C. *Introduction to Engineering Design Optimization*. Prentice-Hall: Englewood Cliffs, NJ, 2000.
75. Kennedy J, Eberhart R. *Swarm Intelligence*. Morgan Kaufmann: Los Altos, CA, 2001.
76. Lagaros N, Papadrakakis M, Kokossalakis G. Structural optimization using evolutionary algorithms. *Computers and Structures* 2002; **80**:571–589.
77. Papadrakakis M, Lagaros N, Thierauf G, Cai J. Advanced solution methods in structural optimisation using evolution strategies. *Engineering Computational Journal* 1998; **15**(1):12–34.
78. Papadrakakis M, Lagaros N, Tsompanakis Y. Structural optimization using evolution strategies and neutral networks. *Computer Methods in Applied Mechanics and Engineering* 1998; **156**(1):309–335.
79. Papadrakakis M, Lagaros N, Tsompanakis Y. Optimization of large-scale 3D trusses using evolution strategies and neural networks. *International Journal of Space Structures* 1999; **14**(3):211–223.
80. Papadrakakis M, Tsompanakis J, Lagaros N. Structural shape optimisation using evolution strategies. *Engineering Optimization* 1999; **31**:515–540.
81. Goldberg DE, Deb K. Special issue on genetic algorithms. *Computer Methods in Applied Mechanics and Engineering* 2000; **186**(2–4):121–124.

DOI: 10.1002/nme